Defence Research and Development Canada | Recherche et développement pour la défense Canada

CAN UNCLASSIFIED

DRDC | RDDC
technologysciencetechnologie

The Empirical Canadian High Arctic Ionospheric Model (E-CHAIM)

Validation and Release

David Themens

P.T. Jayachandran
Anthony McCaffrey
Benjamin Reid
University of New Brunswick

Prepared by:
University of New Brunswick
8 Bailey Drive
P.O. Box 4400
Fredericton (New Brunswick) E3B 5A3
Canada
PSPC Contract Number: W7714-186507/001/SS
Technical Authority: Thayanathan Tayaparan, Defence Scientist
Contractor's date of publication: September 2018

Defence Research and Development Canada
Contract Report
DRDC-RDDC-2018-C185
October 2018

Canada

IMPORTANT INFORMATIVE STATEMENTS

This document was reviewed for Controlled Goods by Defence Research and Development Canada using the Schedule to the *Defence Production Act*.

The Empirical Canadian High Arctic Ionospheric Model (E-CHAIM)

Validation and Release

David R. Themens
University of New Brunswick

P.T. Jayachandran, Anthony M. McCaffrey, Benjamin Reid
University of New Brunswick

Prepared For:
Department of National Defence
DRDC-Ottawa, BLDG 29, 3701 Carling Ave.
Ottawa, Ontario, K1A0Z4, Canada
Contract # W7714-186507/001/SS

The following work is supported through the All Domain Situational Awareness (ADSA) Science & Technology program, contract number W7714-186507/001/SS.

Abstract

This phase of the E-CHAIM project involved the validation and testing of the model in preparation for final release. For this purpose, we first examined the performance of the model under the most extreme conditions one could expect it to operate (intermediate timescales). It is clear from previous work [e.g. Themens et al., 2017a] that E-CHAIM performs well and better than the International Reference Ionosphere (IRI) on monthly median timescales but little has been done to assess the model's performance at shorter timescales. Looking at intermediate (1-to-30-day) timescales we here examine the performance of the E-CHAIM and IRI storm models in accommodating variations at these timescales. Through this work, we demonstrate that, despite the simple nature of the storm parameterization, the E-CHAIM storm model is able to account for 20%-50% of ionospheric variability at intermediate timescales. This, however, is found to be the limit of the operational capacity of empirical models, where only data assimilation can provide further improvement.

To account for the lack of an independent validation of the E-CHAIM topside model in our previous work [Themens et al., 2018], we here present such a validation using Defense Meteorological Satellite Program (DMSP) in situ measurements of electron density. Through this validation we note remarkable improvement in the representation of electron density at DMSP satellite orbit altitudes over the IRI. This improvement is found to be greatest during the summer at high solar activity and can at times exceed a factor of two, while both models provide comparable performance during winter and at low solar activity. In general, E-CHAIM does an excellent job tracking the seasonal behaviour of DMSP electron density in a variety of latitude and local time domains.

In order to assess the capacity of E-CHAIM to be used in HF raytracing applications, we have also applied the model with a PHaRLAP raytracing code. Using this raytracer with E-CHAIM, we note nominal behaviour with no unphysical outliers in the production of simulated vertical and oblique ionograms. Simulations of the Maximum Usable Frequency (MUF) between Resolute and Yellowknife demonstrate largely expected physical behaviour, which we hope to compare to data once available. Comparisons of E-CHAIM-derived receive power and O-mode virtual traces show largely consistent behaviour with a limited set of available oblique ionograms.

Finally, we present a summary of the E-CHAIM code features released coincident with this report.

Significance for Defence and Security

This work sees the conversion of a research, IDL language, E-CHAIM code into a series of operation models including C, Matlab, and IDL versions, as well as a web interface, similar to that of the Internation Reference Ionosphere (IRI). The research conducted under this deliverable sought to extensively validate components of the E-CHAIM that were not independently assessed in the previous deliverables. This work also undertook basic testing of the model in HF communications and ray tracing applications, where we have here compared model-derived

simulations of vertical and oblique ionograms to a limited set of available real data from the Canadian High Arctic Ionospheric Network (CHAIN) and tested the use of the model for identifying Maximum Usable Frequency (MUF) statistics for Canadian high latitude communications links. This work assures the quality and applicability of E-CHAIM toward defense applications, such as Over The Horizon Radar (OTHR) system planning and design.

Résumé

Cette phase du projet E-CHAIM comporte la validation et les essais du modèle précédant la publication de sa version définitive. Dans ce but, nous avons d'abord étudié le rendement du modèle dans les conditions de fonctionnement prévisibles les plus extrêmes, soit les échelles de temps intermédiaire. Nos travaux antérieurs (Themens et coll. 2017a) ont montré qu'aux échelles moyennes mensuelles, qu'E-CHAIM a un bon rendement et donne des résultats supérieurs à ceux de l'ionosphère internationale de référence (IIR), mais nous avons fait peu de travail pour évaluer le rendement sur des périodes plus courtes. Nous nous penchons ici sur les échelles de temps intermédiaires de un à trente jours pour étudier le comportement des modèles de tempêtes d'E-CHAIM et de l'IIR pour tenir compte des variations à ces échelles. Grâce à ce travail, nous démontrons qu'en dépit de la simplicité de la paramétrisation des tempêtes, le modèle de tempêtes d'E-CHAIM peut expliquer entre 20 % et 50 % de la variabilité ionosphérique aux échelles de temps intermédiaires. Nous avons toutefois trouvé que cette paramétrisation limitait la capacité opérationnelle des modèles empiriques qui ne pourront être améliorés que par l'assimilation de données.

Étant donné l'absence d'une validation indépendante du modèle d'E-CHAIM pour le haut de la couche dans nos travaux antérieurs (Themens et coll., 2018), nous présentons une telle validation basée sur les mesures *in situ* de la densité d'électrons par le Defense Meteorological Satellite Program (DMSP) des États-Unis. Cette validation a permis de constater une amélioration remarquable par rapport à celle de l'IIR de la représentation de la densité d'électrons aux altitudes de l'orbite des satellites du DMSP. Nous avons trouvé que cette amélioration était plus grande pendant l'été lors de fortes activités solaires et à certains moments pouvait être d'un facteur deux. Toutefois, les deux modèles ont un rendement comparable en hiver et pendant les périodes de faible activité solaire. En général, E-CHAIM suit très bien le comportement saisonnier de la densité d'électrons trouvée par le DMSP pour un éventail de domaines de latitudes et de temps locaux.

Pour évaluer la capacité d'utilisation d'E-CHAIM avec les programmes de traçage de rayons pour les hautes fréquences, nous l'avons testé avec un logiciel de traçage de rayons PHaRLAP. Nous avons constaté que l'utilisation de ce traceur de rayons avec E-CHAIM produisait un comportement nominal sans données aberrantes non physiques lors de la production d'ionogrammes simulés verticaux et obliques. Les simulations de la fréquence maximale utilisable entre Resolute et Yellowknife montrent un comportement physique largement prévisible que nous souhaiterions comparer avec des données d'observation si elles devenaient disponibles. Les comparaisons entre les puissances reçues calculées par E-CHAIM et les traces virtuelles des ondes ordinaires montrent un comportement en accord général avec l'ensemble limité des ionogrammes obliques disponibles.

Pour finir, nous présentons un résumé des éléments principaux du programme E-CHAIM, publié concurremment avec le présent rapport.

Table of contents

List of figures

List of tables

Acknowledgements

Infrastructure funding for CHAIN was provided by the Canadian Foundation for Innovation and the New Brunswick Innovation Foundation. Science funding is provided by the Natural Sciences and Engineering Research Council of Canada. The authors would like to thank the many ionosonde operators who provided data to this project. This paper uses ionospheric data from the USAF NEXION Digisonde network, the NEXION Program Manager is Mark Leahy. This publication makes use of data from the Qaanaaq and Nord ionosondes, owned by the U.S. Air Force Research Laboratory Space Vehicles Directorate and supported in part by the Air Force Office of Scientific Research. The authors thank Svend Erik Ascanius of the Danish Meteorological Institute and Denmark's Arctic Command for the operation of these ionosondes. This paper uses data from the Juliusruh Ionosonde which is owned by the Leibniz Institute of Atmospheric Physics Kuehlungsborn. The responsible Operations Manager is Jens Mielich. The authors are grateful to Konstantin Ratovski for the operation of the Irkutsk ionosonde. The Tromsø ionosonde is funded in part by QinetiQ.

1 Introduction

The following report presents our work regarding a series of validations of E-CHAIM, as well as provides a series of examples of the model's use in various HF communications applications. Section 2 examines E-CHAIM's performance in modeling electron density at intermediate (1-to-30-day) timescales within the Canadian polar cap. Section 3 undertakes an extensive validation of E-CHAIM against topside in situ electron density obersvations at 830km – 880km from the DMSP satellite constellation. Section 4 presents a series of examples of the use of E-CHAIM in raytracing applications, both with respect to predicting frequency band availability and to reproducing vertical and oblique HF sounding observations. Finally, Section 5 introduces the model code and summarizes the basic model content.

2 Performance at Intermediate Timescales

2.1 Introduction

Empirical models, such as the International Reference Ionosphere (IRI), the NeQuick, or the Empirical Canadian High Arctic Ionospheric Model (E-CHAIM), have demonstrated remarkable performance in providing ionospheric electron density on monthly, or larger, timescales in a variety of environments [Sethi et al., 2008; Ehinlafa et al., 2010; Ezquer et al., 2011; Bilitza et al., 2012; Wichaipanich et al., 2012; Themens et al., 2017a]. At mid latitudes the IRI and NeQuick are widely used in both scientific and operational capacities due to their strong performance in representing climatological electron density variability and their general convenience/simplicity of use [Komjathy and Langley, 1996; Komjathy et al., 1998; Hernandez-Pajares et al., 2002; Bust et al., 2004; Schmidt et al., 2008; Zeilhofer et al., 2009; Pezzopane et al., 2011; Galkin et al., 2012]. At high latitudes local models, such as E-CHAIM and that of Karpachev et al. [2016], have recently been developed for similar purposes and show promise in the representation of expected large-scale ionospheric features, such as the Main Ionospheric Trough (MIT).

The above models all provide quiet time, climatological representations of electron density, while both the IRI [Bilitza and Reinisch, 2008] and E-CHAIM [Themens et al., 2017a] provide supplemental adjustments to their quiet time models to account for storm-time variability. These adjustment models are hereafter referred to as Storm Models. The IRI's Storm Model is that of Aurojo-Pradere et al. [2002a, 2002b], where ap index, integrated over the previous 33 hours with a specially designed filter, is used to drive a linear model of the ratio of perturbed to unperturbed F2-layer critical frequency (foF2). E-CHAIM's Storm Model allows for spatial variations in the ionospheric storm response through the use of a Spherical Cap Harmonic Expansion that is driven by various functions of Dst, ap index, and Auroral Electrojet (AE) index in forms inspired by the work of Wu and Wilkinson [1995] and Perrone et al. [2001].These Storm Models allow the IRI and E-CHAIM to provide a representation of intermediate (1- to 30-day) timescale variations in electron density, which are dominated by ionospheric storm variability.

While validations have shown that these Storm Models provide a measure of improvement over the climatology during ionospheric storms, particularly in the representation of negative storm responses, little has been done to quantify or assess the degree of this performance improvement outside of case studies [Themens et al., 2017a; Aurojo-Pradere et al., 2002a and 2002b]. It is the focus of this study to determine the limitations of these models in their capacity to represent intermediate (1- to 30-day) timescales. To this end, we here attempt to assess the representations of these timescales in one of the most dynamic environments available: the polar cap.

E-CHAIM proposes to provide the best possible empirical representation high latitude ionospheric electron density; however, due to the increased complexity of the environment, the question arises of whether an empirical approach, such as that employed by E-CHAIM or the IRI, is even capable of satisfactorily representing the high latitude ionospheric environment. This concern stems predominantly from the highly dynamic variability of high latitude electron density, which includes manifestations of the transport of plasma from mid latitudes in the form

of a tongue of ionization or patches [Foster et al., 2005], localized or elongated enhancements in electron density due to precipitation [Watson et al., 2011], and various other processes that drive large changes in F-region plasma on minute, hourly, and day-to-day time scales. The high degree of variability at high latitudes on a variety of time scales brings in to question the representativeness of monthly medians as a concept in these regions and thus brings into question the capacity of empirical models to represent these environments.

In this study, we first assess the representativeness of monthly medians at high latitudes in Section 2.3 before then examining the performance of the IRI and E-CHAIM in representing intermediate (1- to 30-day) time scales within the Polar Cap in Section 2.4. We finish with a discussion of the results in Section 2.5.

2.2 Data and Models

2.2.1 The Canadian High Arctic Ionospheric Network (CHAIN)

CHAIN operates a network of six ionosondes and 24 GNSS receiver instruments in the Canadian Arctic, where all six ionosondes are collocated with GNSS receivers [Jayachandran et al., 2009]. A map of the CHAIN network is presented in Figure 1.

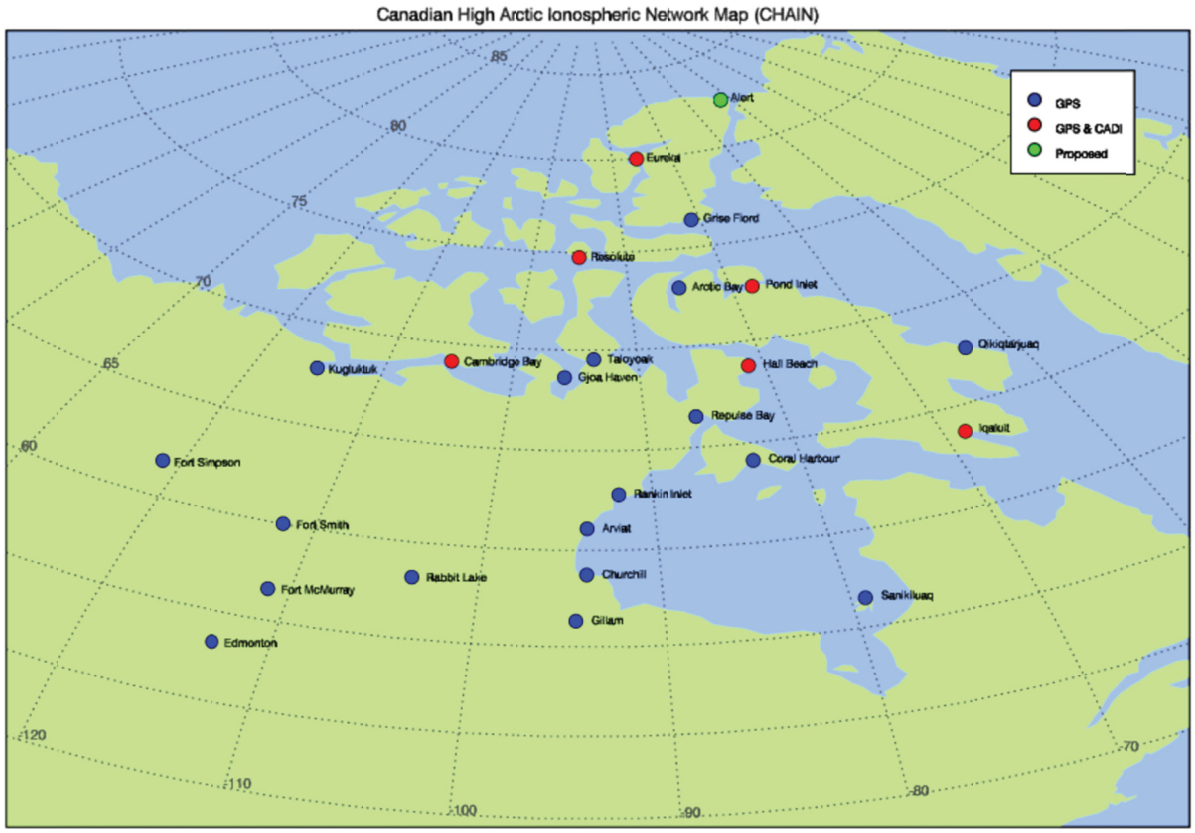

Figure 1. Map of CHAIN station locations. Red dots correspond to locations with both a GPS instrument and ionosonde, blue dots correspond to sites with only GPS receivers, and green dots correspond to proposed future sites.

For this study, approximately 40,00 virtual-height ionograms at Resolute and Cambridge Bay have been manually interpreted (scaled) and then processed into real-height electron density profiles by the POLynomial Analysis (POLAN) procedure of Titheridge [1985, 1988], from which we have here derived the peak electron density of the ionosphere (NmF2). Full-time operation of the CHAIN ionosondes began in 2008 but intermittent observations date back to 1995 for some sites operating under previous programs. Ionograms are available at 5 min temporal resolution up to 2009, after which ionograms are available in 1 min intervals. Ionogram data can be readily accessed via ftp at http://chain.physics.unb.ca. For this particular study, we have only processed the dataset at 30-minute resolution. As the focus of this study is on 1-to-30-day timescales, this temporal resolution should be more than sufficient for our purposes.

2.2.2 E-CHAIM

E-CHAIM is an empirical model of ionospheric electron density, first proposed in Themens et al. [2017a], designed as an alternative to the use of the IRI at high latitudes. The model is now free

and openly available online at http://chain.physics.unb.ca. The E-CHAIM distribution features source code versions provided in Matlab, IDL, and C, as well as a website interface, similar to that available for the IRI. A Python interface is also now under development.

Focusing here solely on NmF2, the seasonal variability of E-CHAIM's NmF2 model uses a Fourier expansion up to triennial terms [Themens et al., 2017a]. For diurnal variations the model uses 24 separate models for each UT hour, with linear interpolation used to define NmF2 between each model. For timescales between these seasonal and diurnal time scales, hereafter referred to as intermediate timescales, E-CHAIM provides a storm parameterization driven by time integrations of Auroral Electrojet (AE) index, ap index, and Dst. The parameterization is provided in detail in Themens et al. [2017a]; however, to summarize, the E-CHAIM storm model accommodates spatial, seasonal, and diurnal variability in its relationship between the driving indices and the ratio between perturbed and climatological NmF2.

2.2.3 The IRI

The IRI is the internationally recognized standard for ionospheric specification [Bilitza et al., 2011], built through a collaboration between International Union of Radio Science (URSI) and the Committee on Space Research (COSPAR) over several decades [Bilitza, 1990; 2001; Bilitza and Reinisch, 2008; Bilitza et al., 2000; 2011; 2012]. The IRI features two peak critical frequency (foF2) models: the URSI and CCIR models. For seasonal variability, each of these models uses linear interpolation between separate monthly foF2 maps, as these models were originally developed as monthly median climatological models. For diurnal variations both models use what is effectively an 8^{th} order Fourier expansion in UTC [Jones and Gallet, 1962]. Between these two timescales, the IRI also features the option to enable a storm time perturbation model aptly named the STORM model. This model is driven by a filtered time integration of ap index and allows only for local time variations in the modeling of the ratio between perturbed and climatological foF2.

2.3 Conceptualizing Monthly Medians at High Latitudes

One of the main focuses of this work is to assess the validity of the application of "monthly medians" to the problem of high latitude electron density. It is well known that high amplitude variations in electron density regularly occur at high latitudes, diverging significantly from median behaviour. The question is, how severe are these deviations and how are these reflected in monthly medians? There is a substantial body of work that has assessed the accuracy of monthly median electron density models in their capacity to represent high latitude monthly medians [e.g. Themens et al., 2014, 2016, 2017b; Bjoland et al., 2016; Makarevich et al., 2015]; however, little work has been done identifying the representativeness of these medians with respect to nominal conditions or on trying to assess the degree of expected deviation about these medians. Makarevich et al. [2015] examined the impacts of significant night time depletions in plasma density in the polar cap, called polar-holes, on the representativeness of monthly median models

(in this case the IRI). The International Telecommunications Union (ITU) provides upper and lower deciles of propagation conditions for HF communications [Wilkinson, 2004]; however, the accuracy of these is limited in their application to high latitudes [Athieno and Jayachandran, 2016]. Aside from the ITU model, the work of Aurojo-Pradere et al. [2005] was perhaps the most comprehensive, having developed statistical distributions of deviations about the monthly mean from global peak critical frequency (foF2) observations. These statistics were prior used to develop the IRI's STORM model. Both of these methods have been suggested for inclusion in the IRI to provide statistical representations of deviations about the mean in the IRI model but have not yet been included.

Here we will take a moment to demonstrate the severity of these deviations about the mean in the polar cap using a year of very high quality ionosonde foF2 observations from 2011 at Cambridge Bay, located on the boundary between the polar cap and auroral oval, and Resolute, located well within the Canadian polar cap. We begin by first presenting the ionosonde measurements and their corresponding monthly median foF2, derived using a 30-day boxcar median filter, in Figure 2. To limit the impact of the edges, we have scaled an additional 30 days prior to January 1st, 2011, and 30 days after December 31st, 2011.

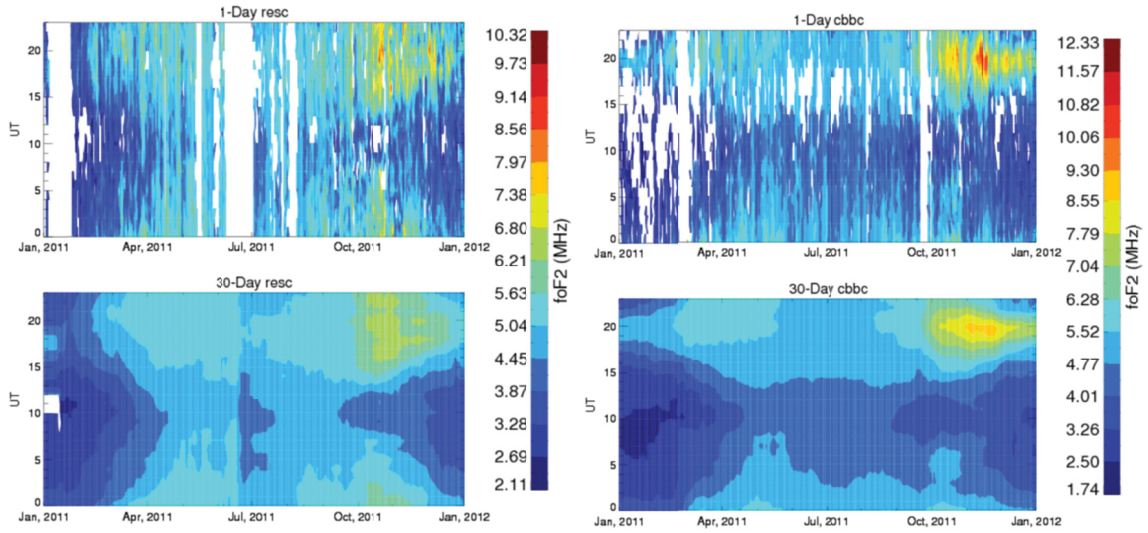

Figure 2. Contours of unfiltered (top) and 30-day-median-filtered (bottom) foF2 at Resolute (left) and Cambridge Bay (right) for 2011.

As you may note, there is significant variability in the unfiltered data that isn't well represented by the monthly medians. For reference, the differences between the monthly median and unfiltered datasets is presented in Figure 3. For illustration purposes and to more easily identify coherent structures in this figure, the data presented in Figure 3 has been smoothed using a 3-day median filter.

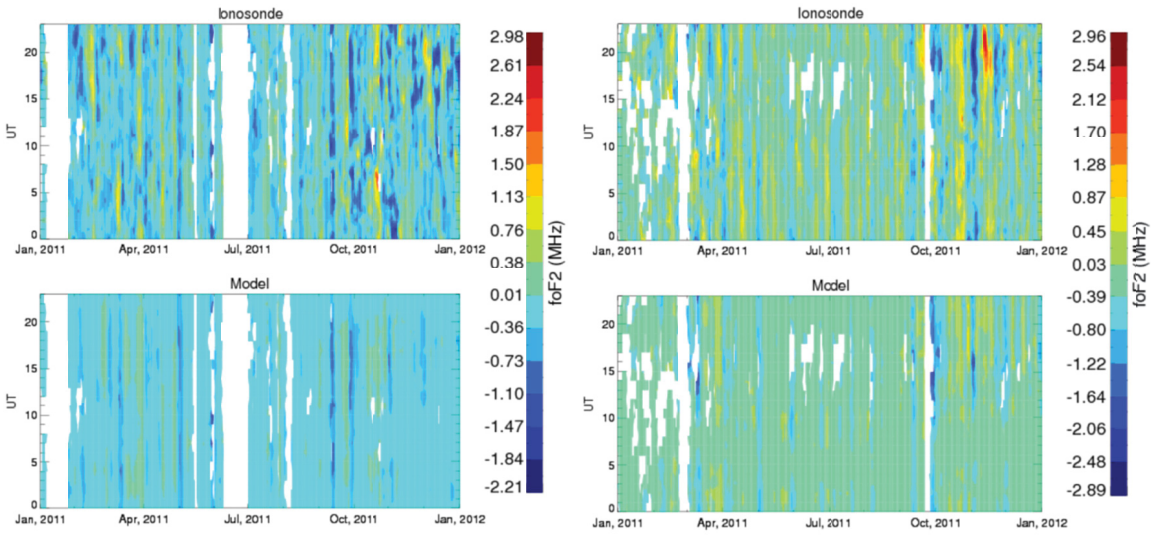

Figure 3. Differences between 30-day median-filtered foF2 and unfiltered foF2 from measurements (top) and E-CHAIM (bottom) for Resolute (left) and Cambridge Bay (right). Positive values imply that the unfiltered foF2 is larger than the 30-day filtered foF2.

Here we clearly see that foF2, at both ionosonde locations, deviates from the monthly median behaviour by several MHz and, at times, peak-to-peak deviations exceed 6 MHz. This level of variability brings us to question the utility of monthly median models in these regions, as 6 MHz variations pose a significant challenge for communications forecasting. Of course, deviations such as these are not entirely localized to high latitudes, resulting in the production of the previously mentioned ITU upper and lower decile models; however, the value of monthly median models decreases as the level of deviation in the environment increases. To provide a measure of the deviation about the monthly median, we have also included plots of the standard deviation about the monthly mean in Figure 4.

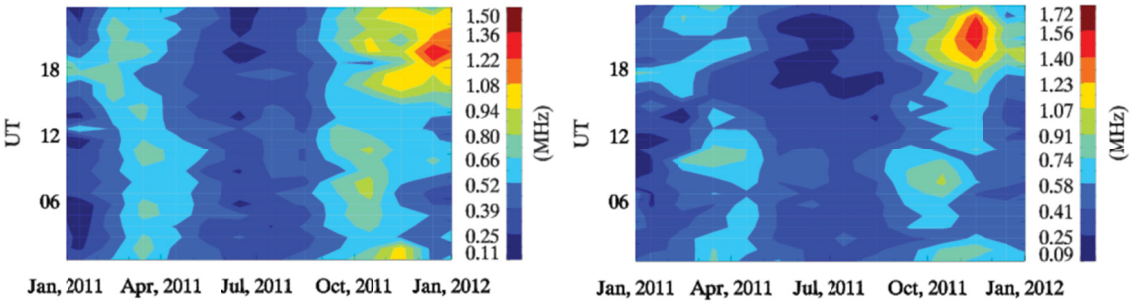

Figure 4. Standard deviations of foF2 about the monthly mean for Resolute (left) and Cambridge Bay (right).

During the summer, we see the standard reduction in ionospheric variability associated with the smoothing of ionospheric gradients by 24-hour sunlit conditions, which culminates in standard

deviations below 0.5MHz at all times [Aurojo-Pradere et al., 2005; Ghezelbash et al., 2014 Or Lamarche and Makarevich, 2015]. That said, during the equinoxes, when patch and storm activity is highest [Sojka et al., 1994; Lyatsky and Hamza, 2001], deviations about the mean can reach as high as 1.7 MHz, well above what is commonly taken as the acceptable standard for foF2 accuracy (1.0 MHz). This implies that models of monthly median foF2 are already incapable of reaching the basic standard, even if their modeled foF2 was perfectly accurate; thus, models of the high latitude environment must provide information on sub-monthly time scales to have any hope of reaching such a standard.

2.4 Representations at Intermediate Time Scales

To represent intermediate (1-to-30-day) timescales, E-CHAIM and the IRI rely on their storm parameterizations. Before proceeding, we first take a moment to return to Figure 3, where we presented the deviation of measured and E-CHAIM-modeled foF2 with respect to their corresponding monthly medians. Despite the significant deviations in the measured foF2, the model appears to qualitatively represent at least a portion of these structures. Of course, it is obvious from this figure that the model is not capturing all of the structuring, nor is it able to capture the magnitude of these deviations. Nonetheless, the challenge is now to quantitatively assess to what extent these variations are capture and to determine what value, if any, is provided through the use of these storm parameterizations.

To evaluate the capacity of these models to represent ionospheric variability on these intermediate timescales, we first conducted a simple experiment whereby we smoothed the measured and modeled foF2 by incrementally larger timescales and compared the resulting smoothed foF2. The results of this simple smoothing comparison are presented in Figure 5.

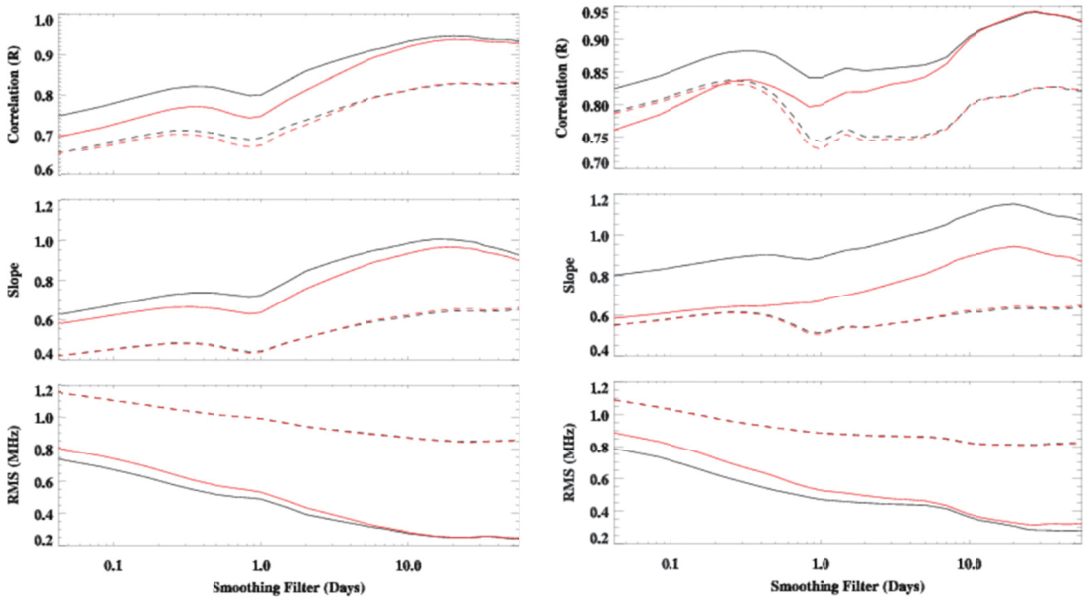

Figure 5. Correlations, linear regression slopes, and RMS differences between measured and modeled foF2 at Resolute (left) and Cambridge Bay (right). The IRI is represented by dashed lines, E-CHAIM is represented by solid lines, quiet time versions of each model are represented by the red curves, and storm versions are represented by the black curves.

Superficially, this figure demonstrates that the storm models are providing an improvement in performance over their quiet-time counterparts at sub-monthly timescales. This is particularly the case for E-CHAIM, where we see improvements over the quiet time model at the measurement timescale by 5% to 10%. Correspondingly, RMS errors of the E-CHAIM storm model are improved by ~0.1MHz over the quiet time model in the un-smoothed comparison. Interestingly, there are characteristically different features in the slope behaviour of the E-CHAIM storm and quiet-time models at Cambridge Bay. We believe that such differences are the result of the fact that Cambridge Bay is at the boundary between the polar cap and auroral oval. Since E-CHAIM models an enhancement in foF2 in the auroral oval, the position of the oval becomes particularly important at Cambridge Bay. The E-CHAIM storm model accommodates for the southward translation of the strong gradient at the auroral oval-polar cap boundary during even modest storms and thus results in a significant improvement in the modeling of foF2 at that location. The presence of this auroral enhancement in the quiet-time model but without accommodating its variation due to geomagnetic activity results in sometimes significant co-location errors in the quiet-time E-CHAIM model, resulting in lower correlations at these timescales than the IRI, which does not represent the auroral enhancement at all. Despite this issue, E-CHAIM demonstrates a systematic improvement over the IRI at all smoothing scales by as much as 0.5MHz at Cambridge Bay and 0.6MHz at Resolute in terms of RMS. This improvement is likely dominated by E-CHAIM's improved performance over the IRI at seasonal timescales.

The above comparison is, of course, limited in the information that it provides, as correlations and slopes in the above comparisons are dominated by diurnal and seasonal variations that empirical models, like E-CHAIM and the IRI, are well equipped to capture. This can be seen clearly by the

significant drop in correlation and slope as one goes from diurnal to daily smoothing scales, associated with the removal of the diurnal variation signal, and the subsequent decrease in correlation and slope as smoothing is increased passed 30 days, associated with the beginning of removing the seasonal signal.

In order to properly isolate the performance of these models on intermediate timescales, we removed the 30-day median-filtered foF2 from each UT hour separately and compared each hour independently. This manner of comparison explicitly removes the diurnal signature and attempts to remove the monthly trend. Since the dataset is not without holes, there are still some artifacts of the data sampling in the resulting comparisons, but since the quiet time versions of the IRI and E-CHAIM have no capacity to model variations on these timescales, we may make use of these versions of the model as a baseline for assessing the validity of this comparison. Deviations between the quiet time model results and the storm model results are thus the focus of the following comparison. The results of this analysis are presented in Figure 6 where we present the model-to-measurement correlations, linear fit slopes, and RMS errors corresponding to the above process.

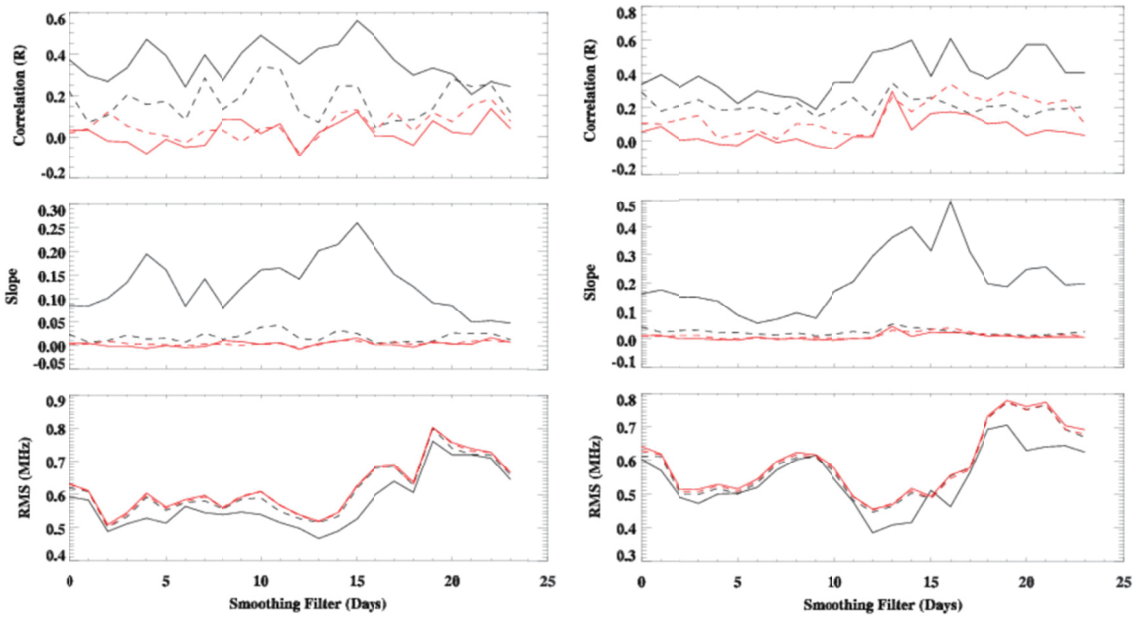

Figure 6. Same as Figure 5 but after removing the 30-day median filtered trend. Left is Resolute, right is Cambridge Bay, black is with storm models turned on, red is with storm models turned off, dashed corresponds to the IRI, and solid corresponds to E-CHAIM.

In Figure 6, we see some minor non-zero correlations in the quiet time model results, likely resulting from data gaps. Regardless, these data gaps do not appear to significantly affect the RMS error or slope comparisons. Looking at the storm model results, we see a systematic improvement in E-CHAIM performance at these intermediate timescales through the use of the storm model, highlighted by improvements in correlation by up to 0.5 at Resolute and 0.3 at Cambridge Bay, improvements in slope by up to 0.25 at Resolute and 0.5 at Cambridge Bay, and improvements in RMS of up to 0.05 MHz at both sites. Interestingly, Resolute sees it greatest

improvements during the morning and evening with larger improvement during night time compared to daytime, while Cambridge Bay sees its largest improvement in the morning and greater improvements during daytime than night time. While the IRI storm model seems to provide a small improvement during nighttime conditions this improvement is limited and does not appear to be significant when examining slopes or RMS errors. This implies that, while the IRI model may be able to represent some of the variability at these timescales, the amplitude of the modeled storm response is significantly underestimated.

2.5 Discussion and Conclusions

It is clear from this study that monthly median models are of limited utility at high latitudes due to the region's high sensitivity to geomagnetic conditions and highly non-linear dynamics. Despite this, simple parameterizations of ionospheric storm perturbations from median behaviour, based on integrated forms of geomagnetic indices, nonetheless appear to have some measure of value. Due to the dominant ionospheric storm response on multi-day time scales at high latitudes being a negative ionospheric response due to composition changes [Fuller-Rowell, 1998], geomagnetic indices, which can often be related to joule heating in a simple manner [Foster et al., 1983; Baumjohann and Kamide, 1984], provide a reasonable measure of information about the resulting storm-perturbation of the ionosphere in these regions over intermediate time scales. On shorter, hourly or day-to-day time scales, patches, tongues of ionization, and other mesoscale ionospheric structures dominate ionospheric variability at high latitudes [Foster, 2005], and due to the complex mechanisms governing the production and transport of these structures, simple relationships to geomagnetic activity indices are ill-suited to representing variability on these daily and sub-daily timescales.

Here the E-CHAIM parameterization demonstrates the capacity to accommodate between 20% and 50% of storm-driven ionospheric variability at intermediate (1-to-30-day) timescales. This, however, only translates into an improvement of 0.05 MHz in terms of overall RMS error, which may not be sufficient to make stand-alone empirical models operationally applicable to high latitude regions. Nonetheless, with overall RMS errors below 0.8 MHz at both sites, E-CHAIM appears to reach the 1 MHz minimum accuracy threshold, at least at these two locations.

In general, while the IRI storm model appears to capture some of the intermediate timescale variability at these locations, the amplitude of the modeled variability is highly underestimated by the IRI and is essentially inconsequentially small. As the IRI Storm model has no dependence on location, this result may highlight the need to accommodate spatial differences in ionospheric storm responses in these models, especially seeing that E-CHAIM, which does allow for spatial variations in this response, appears to significantly outperform the IRI on these timescales.

The aforementioned limitation of these models in no way undermines the utility of these models but, rather, highlights the necessity to assimilate data into these models to see any further improvement. We have here merely presented the capacity limit of these models for representing high latitude electron density variability.

It is clear from the E-CHAIM results that, despite not being able to fully capture intermediate timescale variability, its storm model does provide a measure of value to improving empirical ionospheric representations at these intermediate time scales.

3 Validation Against DMSP in situ Electron Density Data

3.1 Introduction

The Empirical Canadian High Arctic Ionospheric Model (E-CHAIM) is a relatively new empirical representation of high latitude (> 50^{o}N geomagnetic latitude) electron density [Themens et al., 2017a; 2018]. The model was built as a stand-alone replacement for the use of the International Reference Ionosphere (IRI) in these regions and features significant improvements over the IRI in terms of hmF2 and NmF2 [Themens et al., 2017a]. Unfortunately, due to a limited dataset and the desire to use all available topside electron density profiles for the fitting of the model, independent validation of the E-CHAIM topside has not yet been undertaken. It is the intent of this study to provide this independent validation.

Accurate topside electron density modeling is integral to several ionospheric model applications, serving as the dominant contribution to ionospheric total electron content (TEC), particularly at high latitudes [Themens et al., 2014; 2016; Bjoland et al., 2016]. Themens et al. [2016] demonstrated that IRI suffers significant errors in modeling this electron density at high latitudes, sometimes underestimating the integrated topside electron density by up to 6 TECU (1 TECU = 10^{16} e/m^{3}). In that study, the authors demonstrated that, while foF2 errors contributed somewhat to these errors, up to 4TECU of this error stemmed from the topside shape function. These results combined with further diagnostics completed in Themens et al. [2017b] lead the designers of E-CHAIM develop a new topside shape parameterization, built on the successes of the IRI's NeQuick topside function [Coïsson et al., 2006] but modified to provide an improvement in topside curvature and thickness.

While the above changes were demonstrated to provide a significant improvement with respect to the fitting dataset, further validation against independent datasets is necessary. For this purpose, we have here gathered over a decade of in situ electron density observations from the Defense Meteorological Satellite Program (DMSP) constellation of satellites.

In Section 3.2, we provide an overview of the data used in this study and the two models of interest, namely the IRI and E-CHAIM. In this study, we will use the IRI as a baseline standard with which to compare E-CHAIM. In Section 3.3 we present a comparison between DMSP in situ measurements and coincident IRI/E-CHAIM-modeled electron density. We finish in Section 3.4 with a discuss of the results and some conclusions.

3.2 Data

3.2.1 DMSP in situ Electron Density

DMSP satellites orbit in a sun-synchronous, circular orbit at between 830km and 880km with an orbital period of ~110 minutes [Garner et al., 2010]. For this study, due to the redundancy of the orbit of some satellites, we have chosen to only use the F17 and F18 DMSP satellites. This data was gathered from the https://satdat.ngdc.noaa.gov/dmsp/data/ data portal.

DMSP has featured the Special Sensor for Ions, Electrons, and Scintillation (SSIES) instrument package on satellite payloads since the late 1980s. The instruments within this package are jointly capable of determining several plasma properties, the most pertinent to this study being total plasma density (Ne). The main instruments used in this study are the Retarding Potential Analyzer (RPA) and Faraday Scintillation Cup instruments, which are both capable of producing accurate in situ total plasma density (electron density) measurements.

The RPA and scintillation cup instruments are capable of producing a measurement of electron density at 4-second and 24Hz sampling, respectively. Because we are only interested in relatively low-resolution variabilities (both in time and space) and to reduce the overwhelming size of the dataset, we have chosen to only record electron density information every 20 seconds. This sampling resolution translated spatially into a latitude resolution of ~1^{o} and an MLT resolution of better than 15 minutes, where MLT resolutions are greatest at lower latitudes due to the orbit conformation.

To ensure the quality of the dataset, we have undertaken the same quality control measures used in Garner et al. [2010]. This includes their threshold checks of $2 \times 10^{8} < Ne < 10^{12}$ for both the scintillation cup and RPA instruments and their self consistency checks between RPA and scintillation cup measurements for ranging error catching. Please see Garner et al. [2010] for further details. Unfortunately, due to having used the SSIES Environmental Data Record files rather than the binary data, we were unable to undertake the RPA quality control measures that depended on having the raw RPA data.

A plot of the statistical distribution of these the F17 and F18 datasets is presented in Figure 7.

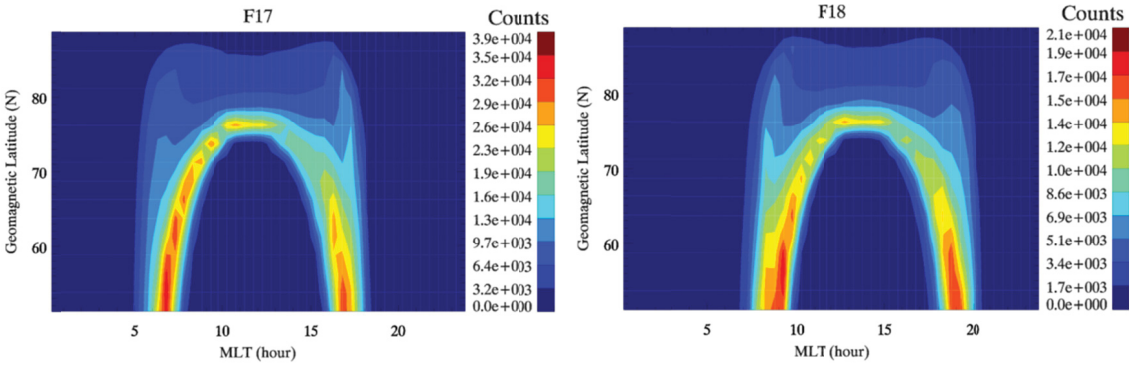

Figure 7. Distribution of DMSP F17 (left) and F18 (right) data with respect to Geomagnetic Latitude and Magnetic Local Time (MLT). For the purpose of these statistics, bins sizes were 0.25 hours in MLT and 2.5o in geomagnetic latitude.

3.2.2 E-CHAIM

The topside and F2-peak components of the E-CHAIM model were first presented in Themens et al. [2017a; 2018]. The model is a regional solution for locations above 50^{o}N geomagnetic latitude and was designed as an alternative to the use of the IRI at high latitudes. The model is now free and openly available online at http://chain.physics.unb.ca. The E-CHAIM distribution features source code versions provided in Matlab, IDL, and C, as well as a website interface, similar to that available for the IRI. A Python interface is also now under development.

E-CHAIM was developed using an extensive dataset of ionosondes, topside sounders, Incoherent Scatter Radars (ISRs), and Radio Occultation (RO) satellites. The topside in E-CHAIM is represented by a modified version of the NeQuick topside function anchored at the F2-region peak density (NmF2) and height (hmF2) [Themens et al., 2018]. The model is fit to basis sets of spherical cap harmonics for spatial variability and Fourier expansions in day of year for seasonal variability. For diurnal variations, the hmF2 and NmF2 models were fit independently for each UTC hour, while the topside thickness model uses local time as its longitude coordinate and functions of solar zenith angle to accommodate its diurnal variability. Both the NmF2 and topside thickness models also feature accommodations for the effect of ionospheric storms.

3.2.3 IRI

The IRI is the internationally recognized standard for ionospheric specification [Bilitza et al., 2011], built through a collaboration between International Union of Radio Science (URSI) and the Committee on Space Research (COSPAR) over several decades [Bilitza, 1990; 2001; Bilitza and Reinisch, 2008; Bilitza et al., 2000; 2011; 2012]. The model features several options for NmF2, hmF2, and topside shape. For the purpose of this study, the Shubin [2015] option was selected for hmF2, as the default AMTB-2013 model was not intended for use above 60^{o}N geomagnetic latitude [Altadill et al., 2013], and the URSI option was selected for foF2, as it is generally found to be the better performing IRI foF2 option at high latitudes [Themens et al., 2014]. The NeQuick option, the IRI's default, was selected for the topside representation.

Based on the results of Themens et al. [2014] and [2018], which demonstrate an underestimation of NmF2 by the IRI and a tendency to overestimate the near-peak topside thickness while underestimating electron density aloft, we expect the IRI's NmF2 and topside thickness errors to negate each other to some extent in the near-peak region but result in an additive underestimation of electron density at high altitudes (beginning above approximately hmF2 + 200km).

3.3 Validating E-CHAIM

3.3.1 Overall Comparison

We begin the process of validating E-CHAIM with DMSP in situ data by first examining the overall distribution of performance over the entire dataset. We realize that this type of comparison can be misleading due to the anisotropic sampling in local time that occurs at the polar portion of the DMSP orbit, but nonetheless present these average statistics to begin our discussion.

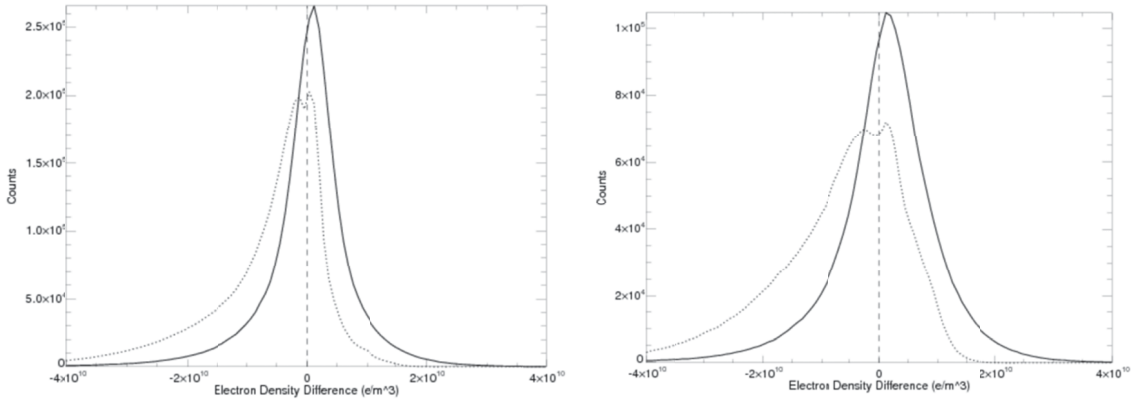

Figure 8. Probability distributions of electron density errors for the IRI (dotted lines) and E-CHAIM (solid lines) with respect to DMSP in situ electron density data for satellite F17 (left) and satellite F18 (right).

From Figure 8 we first note largely symmetric error statistics from E-CHAIM with the peak of the error distribution indicating a slight overestimation trend. For the IRI, we see a highly skewed error distribution toward underestimation with a double peak feature near the distribution maximum. This double peak is likely the result of two separate error populations, the nature of which we will discuss as we further isolate portions of the dataset for more informative comparisons. Regardless, from Table 1 we see that E-CHAIM appears to outperform the IRI on the average when examining RMS errors over the entire dataset.

Table 1. E-CHAIM and IRI Mean and RMS errors for DMSP satellites F17 and F18.

	Mean Error (e/m^3)	RMS (e/m^3)
IRI F17	-6.0E+09	1.2E+10
E-CHAIM F17	2.9E+08	8.3E+09
IRI F18	-6.0E+09	1.3E+10
E-CHAIM F18	8.0E+08	9.8E+09

3.3.2 Morning and Evening Seasonal and Solar Cycle Variations

To better identify the strengths and shortcomings of each model, we will now examine the performance of each model in their representation of monthly averages in a series of isolated domains. Because of the orbital conformation of the DMSP satellites, we note from Figure ___ that the dataset is generally isolated to MLT bands for lower latitudes, but the transit across the

pole leads to a wide variation in MLT at higher latitudes. For the following assessment, we first examine the narrow bands in MLT in two latitude bins (50 - 60°N, and 60 - 70°N geomagnetic latitude) before later proceeding to examine monthly median behaviour in a 70-80°N geomagnetic latitude bin. For satellite F17, the bands of MLT used are 5.5 - 7.5 and 16 - 18 hours MLT. For F18, we examine MLT hours 7.5 - 9.5 and 18 - 20. In Figure 9, we present the monthly average electron density at DMSP orbits for these MLT and geomagnetic latitude bins for satellite F17.

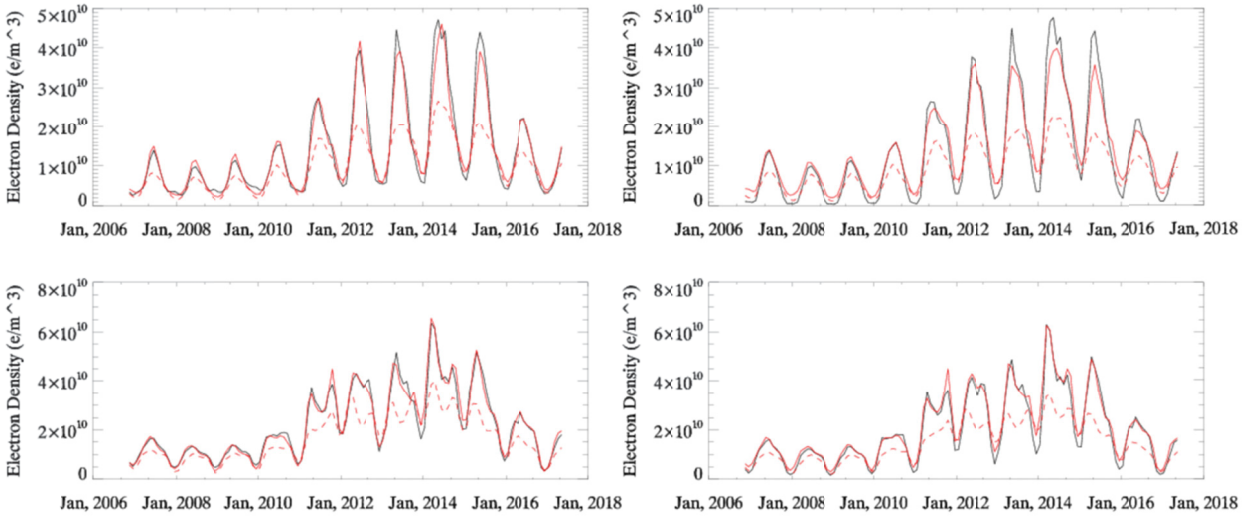

Figure 9. Plots of monthly mean electron density from DMSP F17 (black line) and the E-CHAIM (red solid line) and IRI (red dashed line) models at the DMSP F17 satellite orbit. The top plots correspond to the 5.5-7.5 MLT bin, the bottom plots correspond to the 16-18 MLT bin, the left plots are for the 50-60°N geomagnetic latitude bin, and the right plots are for the 60-70°N geomagnetic latitude bin.

From this figure, one can clearly see that the main improvement of E-CHAIM over the IRI is due to E-CHAIM's increased capacity to represent the seasonal variation in electron density along the DMSP orbit. We see that E-CHAIM does an excellent job matching the monthly average electron density trend of the DMSP data, with particular improvement during summer periods and at high solar activity. The IRI fails to capture the amplitude of the seasonal and solar cycle trend in the DMSP observations, generally underestimating electron density during summer and equinox periods, particularly at high solar activity. For the morning MLT bins (5.5 - 7.5 MLT) we note a slight tendency for E-CHAIM to underestimate electron density during summer periods at high solar activity, particularly in the higher latitude bin (60 - 70°N geomagnetic latitude), and converge to the IRI trend of overestimating the electron density during winter periods in the higher latitude bin. For the evening MLT bins (16 - 18 MLT), we note almost perfect performance by E-CHAIM at both latitudes during summer and equinox periods with again a slight tendency to overestimate electron density during the winter, converging to the IRI curve. The IRI appears to again underestimate summer and equinox electron density but also somewhat exaggerates the semi-annual anomaly at high solar activity.

In Figure 10, we present the same monthly averages of Figure 9 but for satellite F18.

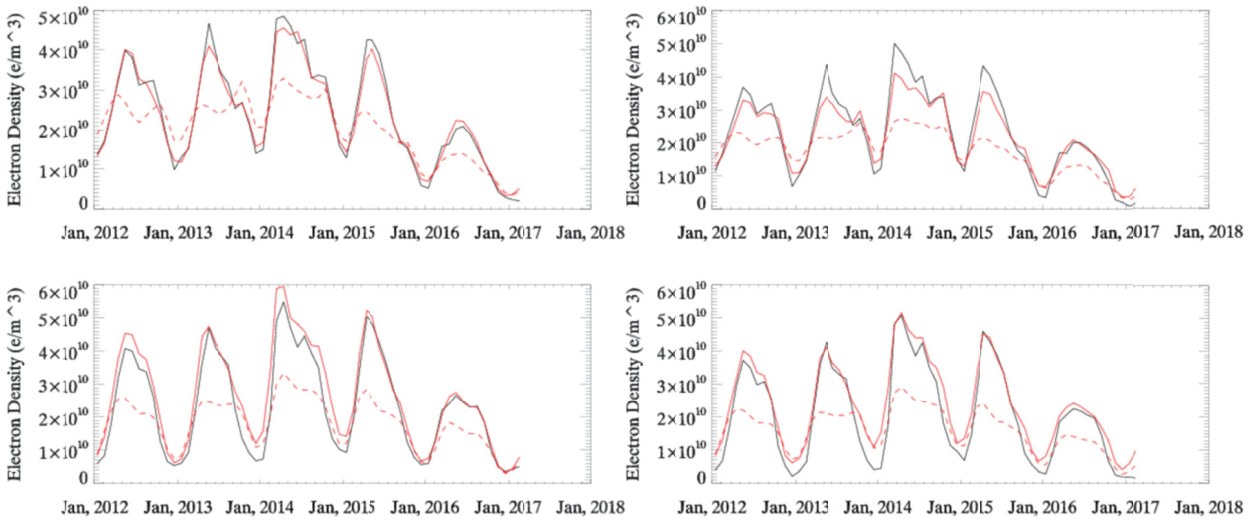

Figure 10. Same as Figure 9, but for DMSP satellite F18. The top plots correspond to the 7.5-9.5 MLT bin, the bottom plots correspond to the 18-20 MLT bin, the left plots are for the 50-60^{o}N geomagnetic latitude bin, and the right plots are for the 60-70^{o}N geomagnetic latitude bin.

As you may note, both E-CHAIM and the IRI again provide similar electron densities during winter periods, culminating in a slight overestimation with respect to DMSP data, but E-CHAIM again significantly outperforms the IRI during summer and equinox periods in all MLT and geomagnetic latitude bins. Overall, the results for satellite F18 are very similar, qualitatively, to those from satellite F17.

To better assess the performance of each model, we also provide the monthly RMS errors corresponding to the data in Figure 9 and Figure 10. These RMS errors are provided in Figure 11 and Figure 12.

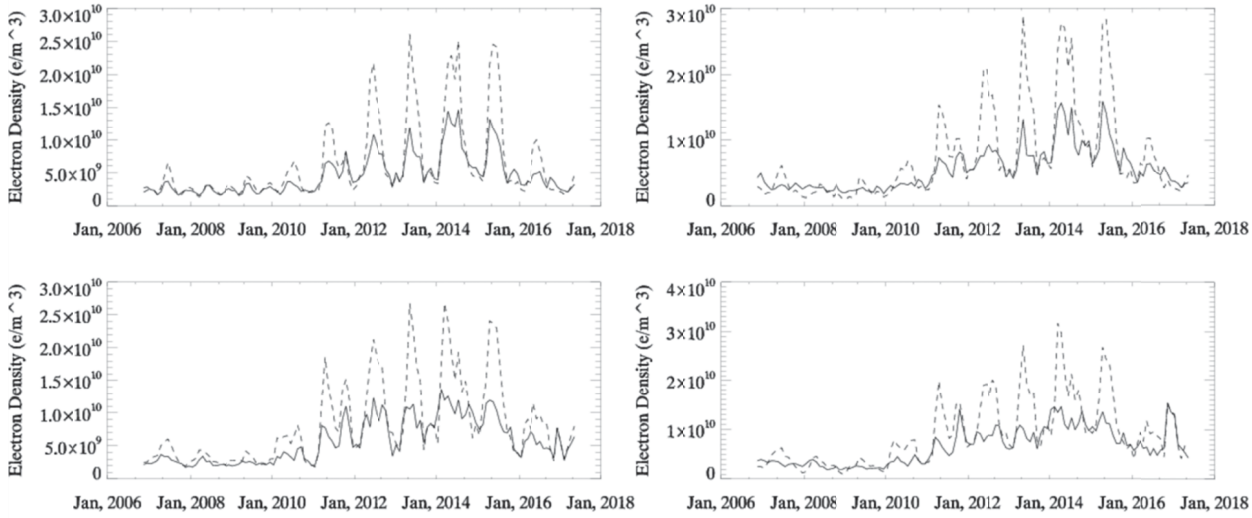

Figure 11. Monthly RMS errors in E-CHAIM (solid lines) and IRI (dashed lines) electron density at the DMSP F17 satellite. The top plots correspond to the 5.5-7.5 MLT bin, the bottom plots correspond to the 16-18 MLT bin, the left plots are for the 50-60^{o}N geomagnetic latitude bin, and the right plots are for the 60-70^{o}N geomagnetic latitude bin.

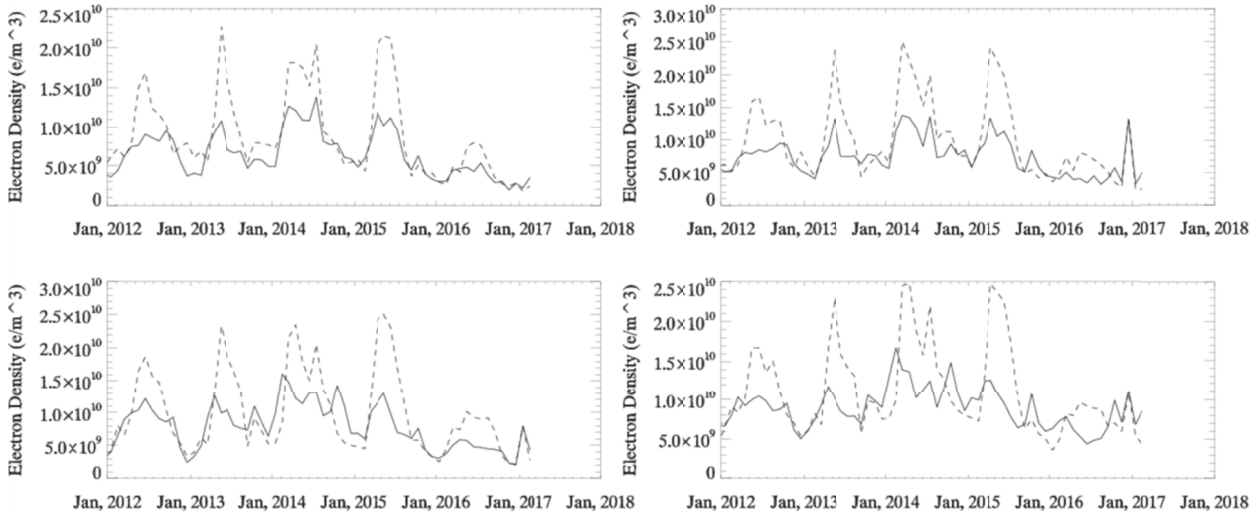

Figure 12. Same as Figure 11 but for DMSP satellite F18. The top plots correspond to the 7.5-9.5 MLT bin, the bottom plots correspond to the 18-20 MLT bin, the left plots are for the 50-60^{o}N geomagnetic latitude bin, and the right plots are for the 60-70^{o}N geomagnetic latitude bin.

Overall, the RMS errors are consistent with our observations based on Figure 9 and Figure 10. We see that E-CHAIM performs better than the IRI, sometimes by a factor of two or more, during summer periods. During winter periods, both models perform comparably, with the IRI performing slightly better during the winter of the declining phase of the last solar cycle. During

solar minimum, both models perform comparably. In general, the errors from both models are greatest during summer periods at high solar activity and are lowest at low solar activity.

3.3.3 Monthly Median Variability in the Polar Cap/Auroral Oval

As the footprint of DMSP spans a wide range of MLTs at high latitudes, we have opted to approach comparisons in a slightly different manner. In Figure 13 we present monthly median electron density from DMSP, E-CHAIM, and the IRI for all available data in a geomagnetic latitude bin of 70 - 80°N from satellite F17.

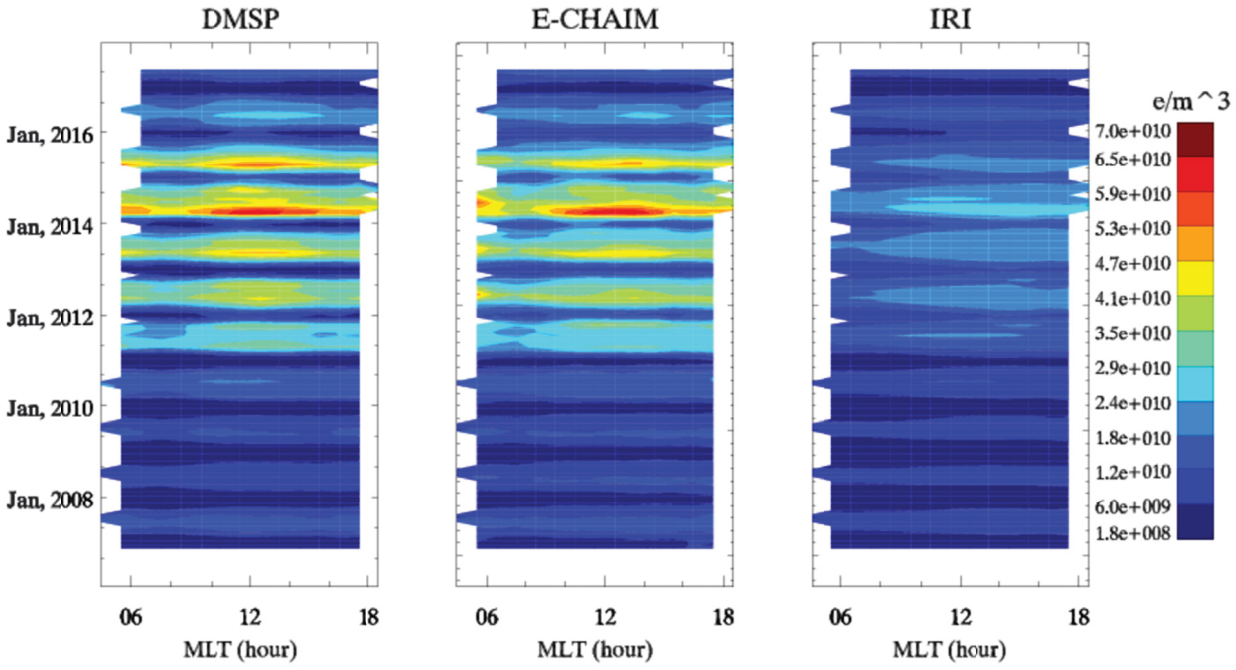

Figure 13. Monthly median electron density from DMSP satellite F17 (left) and corresponding electron density from E-CHAIM (middle) and the IRI (right).

Corresponding plots of the measured and modeled electron density for DMSP satellite F18 are presented in Figure 14.

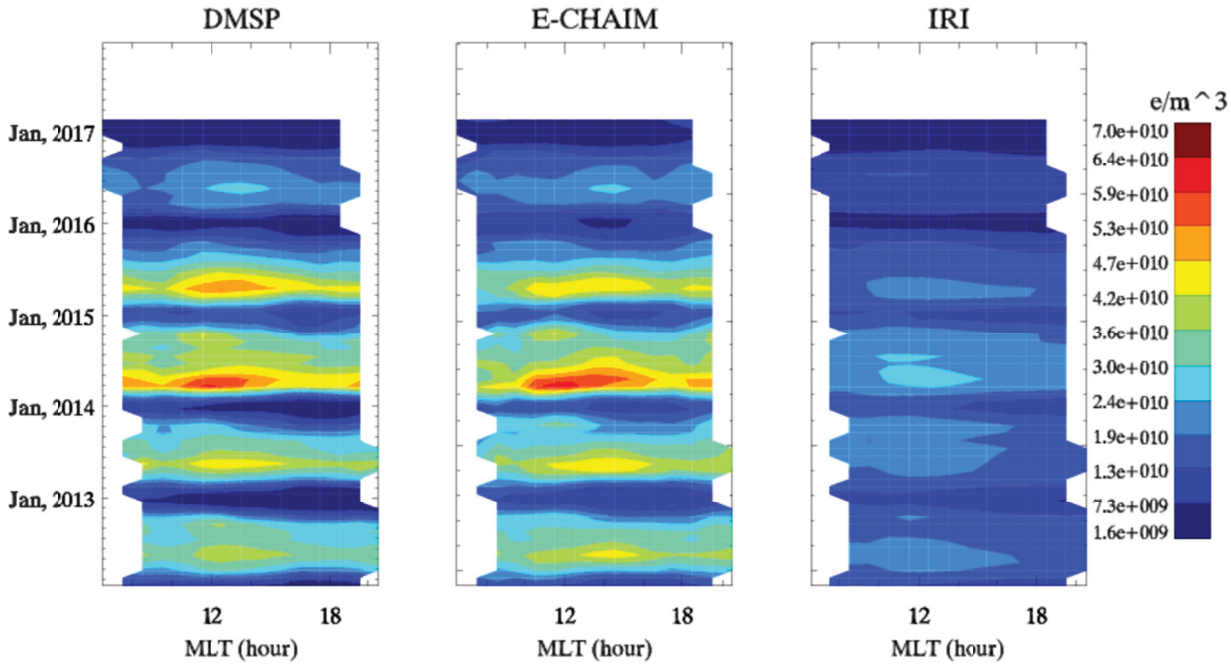

Figure 14. Same as Figure 13 but for DMSP satellite F18.

From Figure 13 and Figure 14 we see that E-CHAIM qualitatively does an excellent job at replicating DMSP F17 in situ electron density, capturing the amplitude and structure of the DMSP observation variability. The IRI however, again appears to significantly underestimate electron density at the DMSP orbit across all MLTs. To more quantitatively assess the model errors, we also present the corresponding monthly RMS errors for satellites F17 and F18 in Figure 15 and Figure 16, respectively.

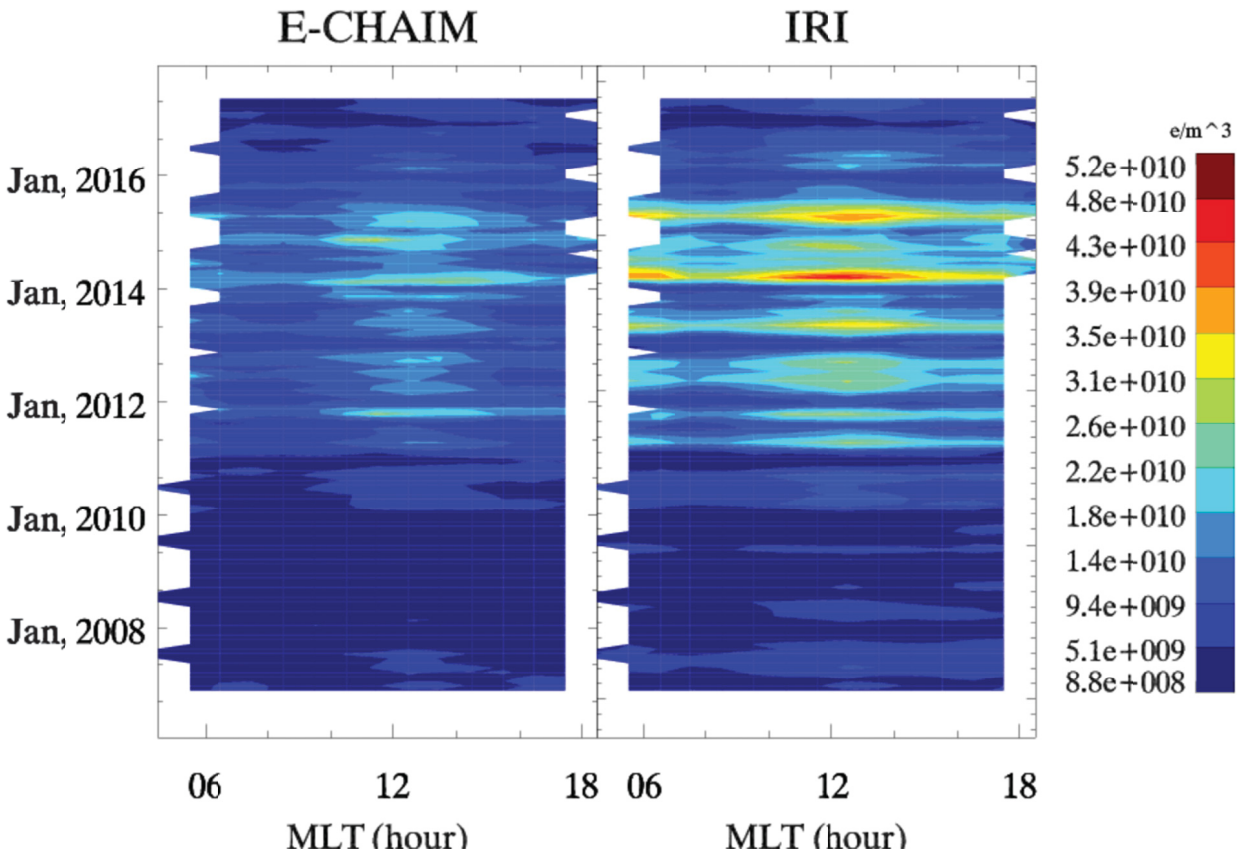

Figure 15. Monthly RMS errors for E-CHAIM (left) and the IRI (right) for satellite F17.

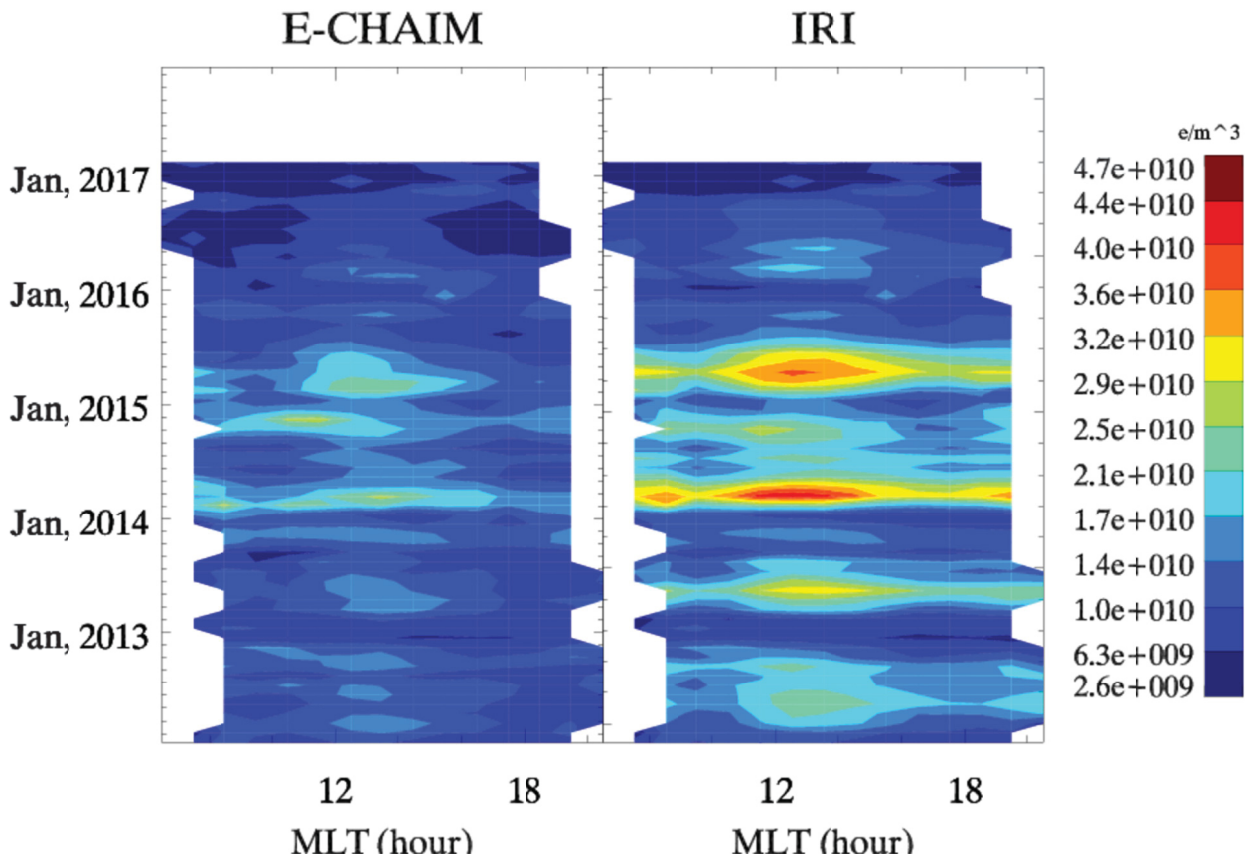

Figure 16. Same as Figure 15 but for DMSP satellite F18.

From these figures, we note that both the IRI and E-CHAIM suffer their largest errors around local noon, particularly during the sudden increases in solar activity of late 2011 and early 2014. Seasonally, both models demonstrate largest errors during the equinoxes, where IRI errors exceed those of E-CHAIM by 50% to 120% at high solar activity but are comparable to E-CHAIM at low solar activity.

3.4 Discussion and Conclusions

As mentioned in Section 3.2.3, based on the evaluations of the IRI that demonstrated a tendency for the topside shape to over estimate electron density in the near peak and underestimate electron density at altitudes above approximately hmF2 +200km [Themens et al., 2018], as well as the tendency for the IRI to underestimate high latitude electron densities [Themens et al., 2014], we expected the IRI to underestimate electron density at DMSP altitudes. This prediction appears to have been proven correct, as the IRI has been here found to nearly universally underestimate high latitude electron density at 830-880km altitudes. For E-CHAIM, their topside model that modified the NeQuick topside model parameterization to better represent the curvature of the high latitude topside profile and their tendency to generally provide more accurate NmF2 at high

latitudes [Themens et al., 2017a] seems to have here culminated in strong overall performance in representing high latitude electron density in the 830-880km altitude range. For both DMSP satellites tested here, E-CHAIM produced an improvement over IRI RMS errors by 3.2 - 3.7 x 10^9 e/m^3 (25% to30%) and appears to qualitatively well capture the seasonal behaviour of DMSP in situ electron density. Based on the combined comparisons of DMSP satellites F17 and F18, the observed improvement appears to span across all magnetic local times. Nonetheless, there remain some appreciable errors in E-CHAIM electron density during winter periods at low solar activity, where performance is comparable to, but sometimes worse than, the IRI. In fact, even for periods where E-CHAIM significant outperforms the IRI, errors can still reach as high as 20%. The task, of course, remains in identifying where these remaining errors are coming from within E-CHAIM, whether it be in hmF2, in NmF2, or in the topside shape function. Further assessment is necessary using either independent, full electron density profile data or more in situ satellite data at varying altitudes in order to full diagnose these errors.

4 Examining the use of E-CHAIM for HF Raytracing

4.1 Introduction

One of the primary applications of E-CHAIM will be as a background model for HF raytracing, particularly for the task of system design and frequency selection for potential OTHR deployments to high latitudes; as such, we feel it necessary to provide some examples of E-CHAIM being applied in such a manner and to conduct some raytracing comparisons to existing datasets.

In Section 4.2 we will introduce the ray tracing code used for the following analysis and briefly summarize the E-CHAIM bottomside representation. In terms of analysis, we first take a moment to examine the behaviour of the maximum usable frequency of an HF radio link between Resolute and Yellowknife in Section 4.3. Following this, we compare a limited number of measured oblique ionograms to simulated oblique ionograms from E-CHAIM in Section 4.4.

4.2 Data

4.2.1 E-CHAIM

E-CHAIM is a regional empirical electron density solution for locations above 50^{o}N geomagnetic latitude and was designed as an alternative to the use of the International Reference Ionosphere (IRI) at high latitudes [Themens et al., 2017a; Themens et al., 2018]. The model is now free and openly available online at http://chain.physics.unb.ca. The E-CHAIM distribution features source code versions provided in Matlab, IDL, and C, as well as a website interface, similar to that available for the IRI. A Python interface is also now under development.

E-CHAIM was developed using an extensive dataset of ionosondes, topside sounders, Incoherent Scatter Radars (ISRs), and Radio Occultation (RO) satellites. The bottomside in E-CHAIM is represented by a single semi-Epstein layer function with a vertically parameterized scale height designed to capture the variations in bottomside density associated with changes in F2-layer thickness, as well as variations in the F1-layer and E-region. The model is fit to basis sets of spherical cap harmonics for spatial variability and Fourier expansions in day of year for seasonal variability. For diurnal variations, the hmF2 and NmF2 models were fit independently for each UTC hour, while the components of the bottomside model use local time as its longitude coordinate and functions of solar zenith angle to accommodate its diurnal variability. Both the NmF2 and the bottomside parameterization models also feature accommodations for the effect of ionospheric storms.

4.2.2 Hall Beach-Iqaluit Oblique Ionograms

In May 2011, the Canadian High Arctic Ionospheric Network (CHAIN) undertook a brief experiment to test their Canadian Advanced Digital Ionosondes (CADI) in an oblique sounding operational mode. During this period, a transmitter at Hall Beach was synchronized to a receive-only station in Iqaluit. While the antenna conformation was not ideal for this application, leading to low power, some clear oblique ionograms were able to be recorded. For this study, we will examine these limited oblique ionograms and compare them to simulations using PHaRLAP, using E-CHAIM as the background electron density model.

4.2.3 PHaRLAP

PHaRLAP is a full-featured ray tracing toolkit developed by Australia's Defence Science and Technology Organisation (DSTO) [Cervera and Harris, 2014]. The toolbox is a robust raytracing software based on the Hamiltonian approach of Haselgrove [1963] with an explicit solution for the group refractive index using the Appleton-Hartree Equation. The software is capable of providing independent solutions for the ordinary and extraordinary modes and determines absorption losses to transmission using the method of George and Bradley [1974], with plans to upgrade the absorption code to an explicit solution called the Semiempirical Model for Ionospheric Absorption based on the NRLMSISE-00 atmospheric model (SiMIAN) [Pederick and Cervera, 2014].

4.3 Frequency Planning: Resolute to Yellowknife

One main applications of E-CHAIM will be its use as a background model in determining the maximum usable frequency on HF links in the Canadian Arctic. To demonstrate the model's capacity in such an application, we have generated oblique incidence ionograms between a theoretical transmitter at Resolute and receiver at Yellowknife for every hour in 2011. In Figure 17 we present the maximum usable frequency from these simulations.

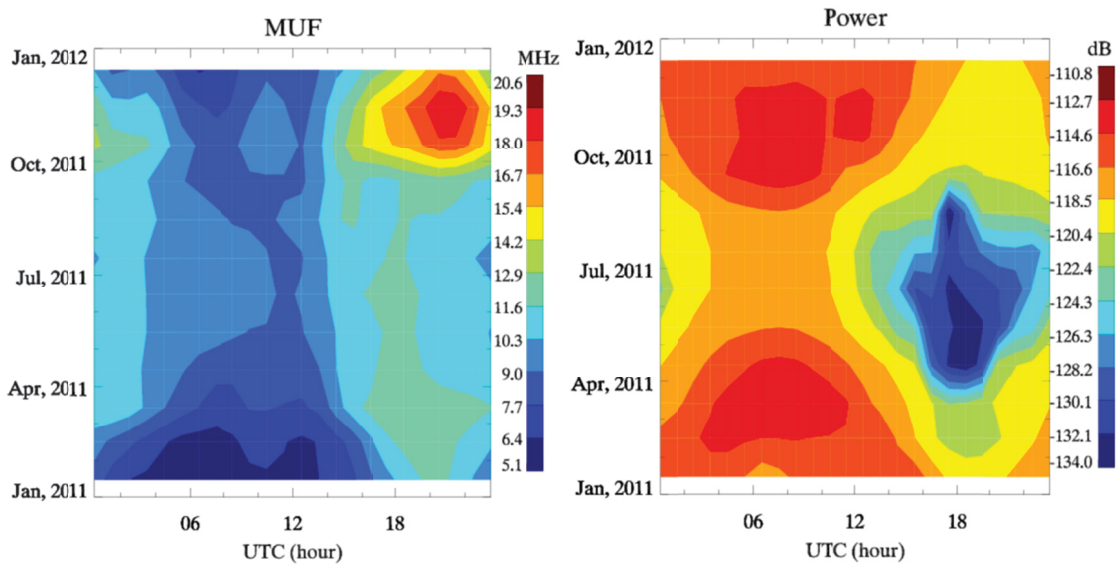

Figure 17. Monthly median MUF (left) and power at MUF (right) for HF links between Yellowknife and Resolute in 2011.

MUFs monthly median MUFs on the link between Yellowknife and Resolute range from ~5 to ~20 MHz, with MUFs peaking during the equinoxes for daylight periods and during the summer for nighttime conditions. From October to December 2011, we note a substantial increase in MUF associated with a short-term increase if solar flux that has been previously reported in Themens et al. [2016] and [2017a]. In the absence of this short-term feature, MUFs generally stayed within the 5.0 to 13.0 MHz range. In terms of received power at the MUF frequencies, we see largely expected trends with received power lowest during summer daytime periods. Less expected are the maxima in transmit power during the equinox nighttime conditions, likely associated with both lower electron density and collision frequencies in the D-region, as well as a reduced geometric path (i.e. less oblique propagation) through the D-region during these periods due to hmF2 reaching local maxima at these times.

4.4 Comparisons to Ionograms

Prior to examining the use of E-CHAIM with respect to oblique ionograms, we first take a moment to examine the behaviour of the model under vertical propagation conditions and compare to these results to vertical ionograms. An example of a manually scaled O-mode trace from the Cambridge Bay CHAIN CADI system is presented in Figure 18 with a superimposed virtual O-mode trace generated using PHaRLAP with E-CHAIM.

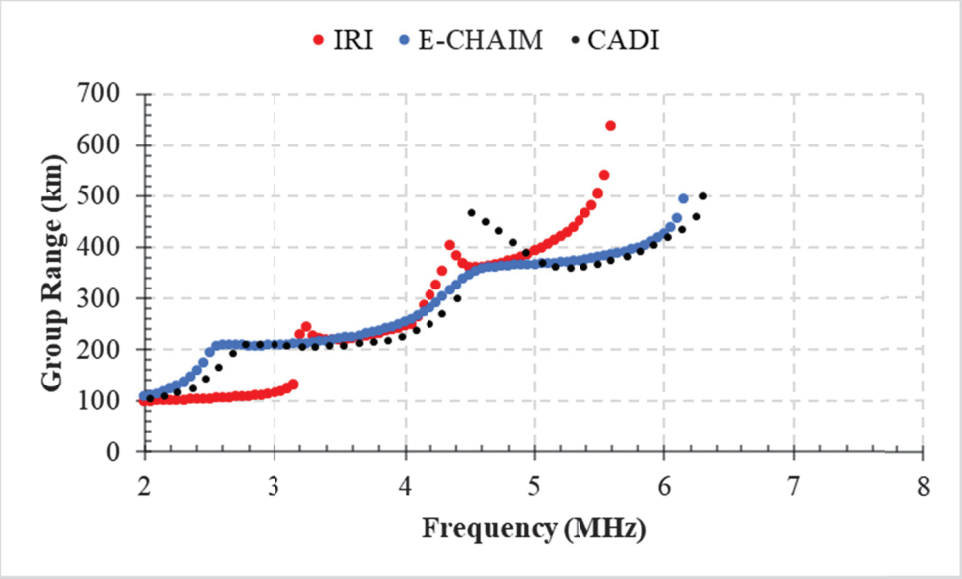

Figure 18. O-mode trace of a CADI ionogram (black) and from E-CHAIM- (blue) and IRI-based (red) raytracing for June 1st, 2014, at 20:00UTC.

There is little need to spend much time focusing on vertical propagation comparisons, as prior comparisons to hmF2 and foF2 at these sites already provide a reasonably clear case for the capacity of E-CHAIM versus other empirical models. That said, those types of analysis are not as sensitive to small errors in the vertical gradients in electron density as tends to be the vase for virtual height profiles. For example, examining Figure 18, we see that E-CHAIM does an excellent job in capturing the foF2 and even the virtual height profile curvature of the F1- and F2-layer traces; however, the model fails to reproduce the strong retardation cusp behaviour found in the virtual height ionogram trace in the transition between the F1- and F2-layers. The challenge here is that even small changes to the gradient in electron density at the cusp of the F1-layer will lead to very different retardation behaviour in that cusp region. This ignores the fact that raytracers are often inaccurate in regions of strong vertical gradients due to the asymptotic behaviour of the refractive index in these regions and some of this strong cusp behavior could be the result of a tilted ionospheric layer, both of which are a serious technical challenge to address. Regardless, E-CHAIM appears to perform well in application with PHaRLAP but does exhibit a tendency to slightly underestimate the critical frequency of the E-region peak.

Before comparing E-CHAIM and PHaRLAP-generated oblique traces to real ionogram data, we will first examine the behaviour of the model in its application to oblique raytracing. In Figure 19 we present examples of the simulated system power on a Hall Beach-to-Iqaluit link on May 2nd, 2011, at 00:14UTC and on May 5th, 2011, at 3:56UTC.

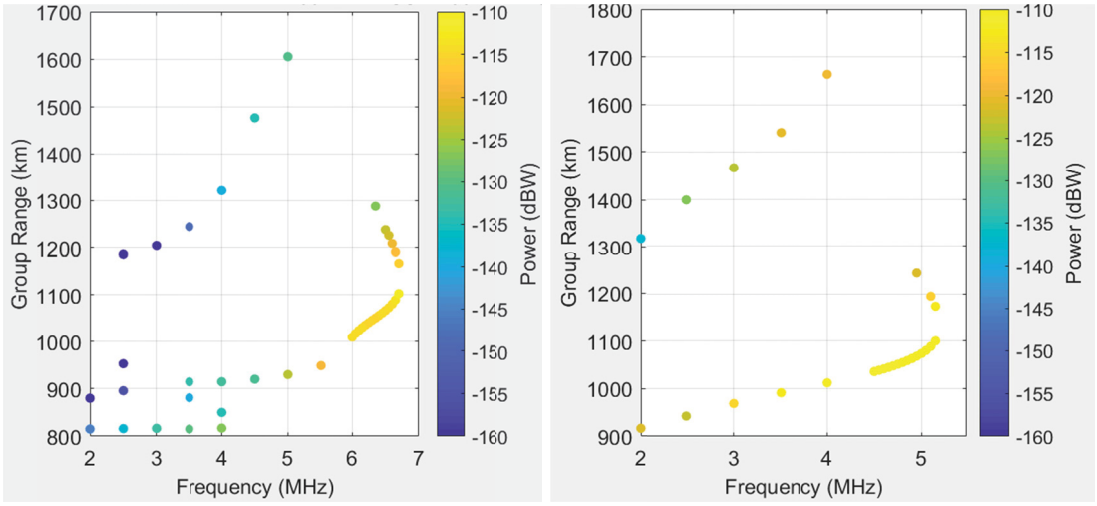

Figure 19. E-CHAIM and PHaRLAP simulated oblique O-mode ionograms between Hall Beach and Iqaluit on May 2nd, 2011, at 00:14UTC (left) and May 5th, 2011, at 3:56UTC (right). Simulations are for a unity gain isotropic receiver and transmit conformation.

From this figure, we note significant signal loss for most echoes below the F-region during the daytime (00:14UTC) simulation. For the nighttime period (3:56UTC), there is less absorption and appreciable signal is simulated for a potential 2-hop mode link. This suggests that any oblique ionograms we do receive at Iqaluit during daytime periods will likely be highly attenuated, partial ionograms. An example ionogram from this 00:14UTC link is presented in Figure 20, where we demonstrate the received power.

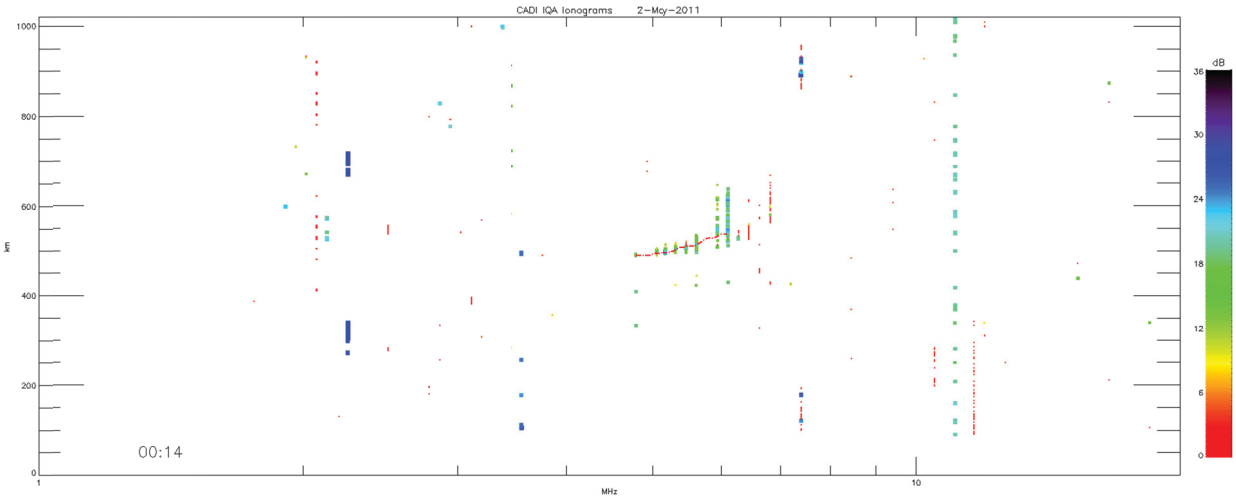

Figure 20 An oblique ionogram recorded at the CHAIN Iqaluit ionosonde at 00:14UTC on May 2nd, 2011. Note that the y-axis here is group range divided by a factor of two, unlike Figure 19.

This figure demonstrates much of what we expected: a highly attenuated partial ionogram. Nonetheless, we see in this figure a clear F2-region trace with a well-defined cusp. Similarly, in Figure 21, we present an ionogram corresponding to the May 5th, 2011, 3:56UTC simulation of Figure 19.

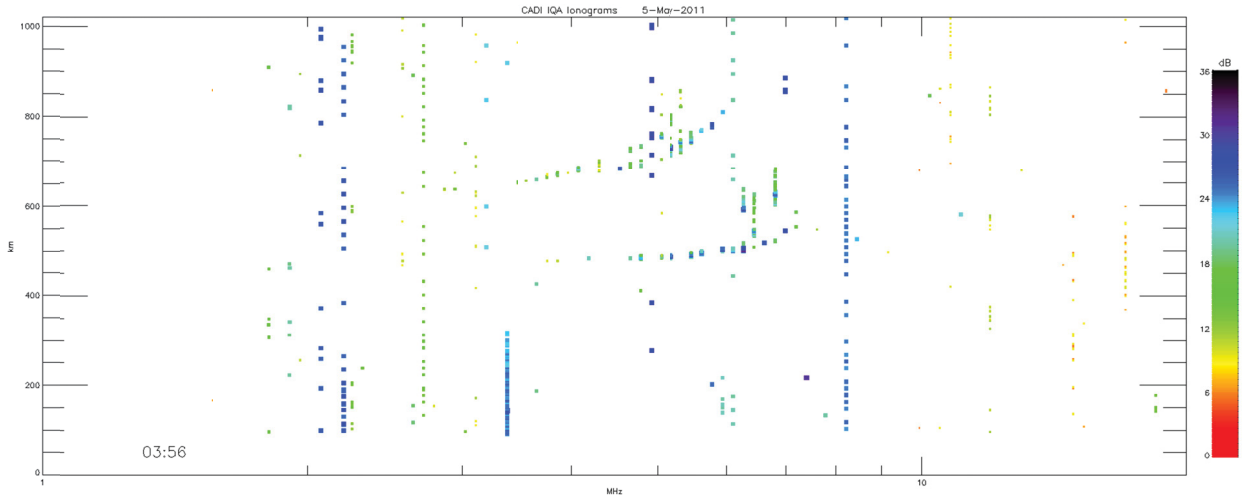

Figure 21. An oblique ionogram recorded at the CHAIN Iqaluit ionosonde at 3:56UTC on May 5th, 2011. Note that the y-axis here is group range divided by a factor of two, unlike Figure 19.

Here we note clear 1-hop and 2-hop modes, largely in agreement with the simulation of Figure 19. In Figure 22, we examine our first example of oblique O-mode traces manually retrieved from CHAIN CADI ionograms over the Hall Beach-Iqaluit link and directly compared to E-CHAIM simulation output for May 2nd, 2011, at 00:14UTC.

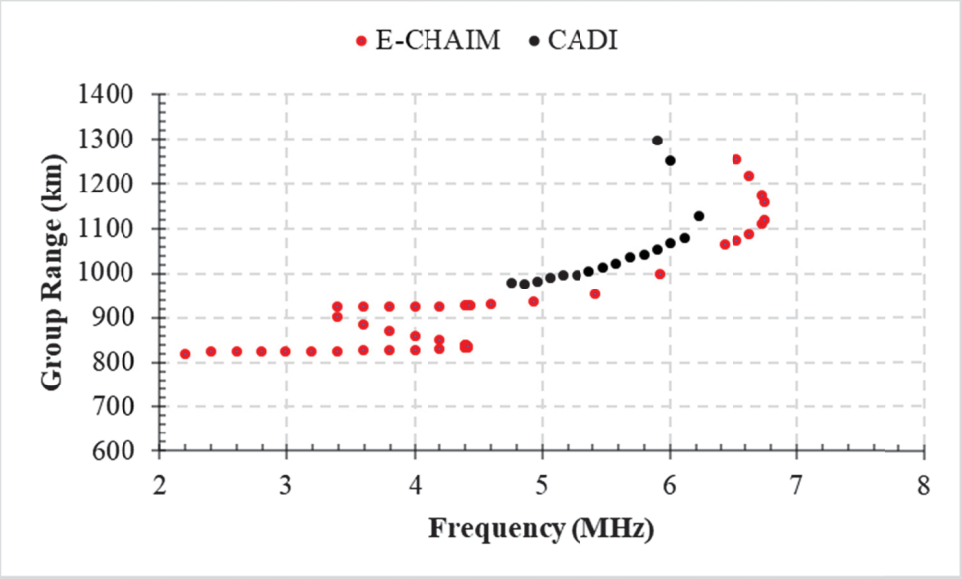

Figure 22. The O-mode oblique ionogram trace recorded at Iqaluit on May 2nd, 2011, at 00:14UTC (black dots) and the corresponding E-CHAIM-PHaRLAP simulated O-mode oblique trace (red dots). No power filtering has been applied to the E-CHAIM-PHaRLAP simulated trace.

This figure shows relatively good agreement between the CHAIN CADI trace and the E-CHAIM-derived trace, with E-CHAIM demonstrating a slight overestimation of the MUF (~0.5MHz), which is understandable given that this period corresponds to geomagnetic storm conditions. A second oblique ionogram example is provided in Figure 23, where we will note both an F-layer and E-region trace.

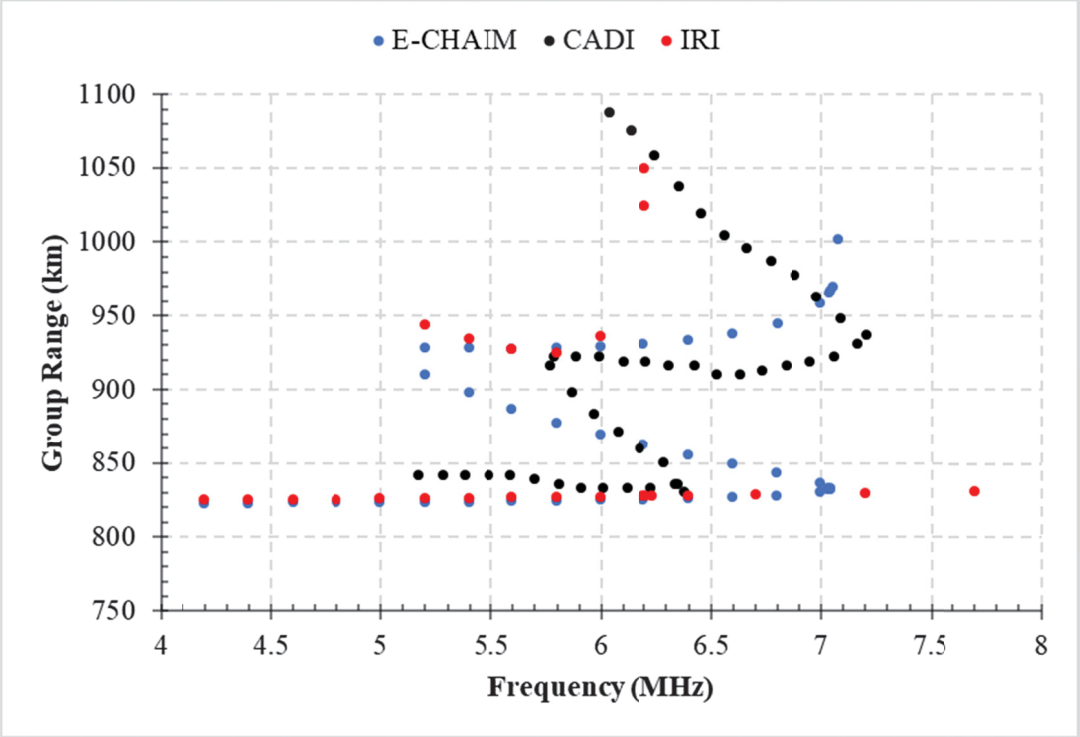

Figure 23. The O-mode oblique ionogram trace recorded at Iqaluit on May 22nd, 2011, at 11:58UTC (black dots) and the corresponding E-CHAIM (blue dots) and IRI (red dots) PHaRLAP-simulated O-mode oblique traces.

The ionogram traces of Figure 23 correspond to quiet geomagnetic conditions. In this case, we see good agreement between E-CHAIM and CADI F-layer MUF but a tendency for the E-CHAIM simulation to overestimate the E-Region MUF. In this figure, we have also provided the simulated trace generated using the IRI. You'll note the IRI's further overestimation of the E-Region MUF, absence of cusp echoes, and underestimation of the F-Region MUF

Overall, based on the above examples and extensive testing in our previous research, we believe that E-CHAIM is well suited to being used as a background model for HF raytracing.

5 Public Release of the E-CHAIM Codes

As part of this deliverable, we have taken the original E-CHAIM research code and produced an operational model distribution. The model features four versions:

1) An IDL version.
2) A Matlab version that manages a self-updating local database.
3) A Matlab version that uses a daily updated, CHAIN-generated, database (called the C database).
4) A C code that uses the same C database.

In terms of features, each code is capable of generating full electron density profiles or in situ "satellite" single point electron density measurements. The codes are each also capable of generating NmF2, hmF2, hmF1, NmF1, and NmE (note, hmE = 102km in E-CHAIM) at the user's request. Also, for ease of use by our client, the Matlab version of the code includes two additional features, not included in the other model versions:

a) A "map" mode used for generating a four-dimensional data cube without the need for additional effort on the user's part.
b) A Graphic User Interface (GUI) that can generate profiles, time series, or contours that can be outputted in independent plot windows, in a graphic list format, or exported as an ASCII file.

In addition to the above versions of the model, we have also developed a web interface version of the model hosted on the CHAIN webserver. This web interface is similar in concept to that of the International Reference Ionosphere (IRI) but functions in an identical manner to the Matlab GUI interface.

All versions of the E-CHAIM codes can be found on the E-CHAIM website at https://e-chaim.chain-project.net While the E-CHAIM web interface is openly accessible without the need for additional credentials, the source code download page requires the creation of an account. These accounts are not actively monitored and are automatically authorized. They exist solely to help the project team communicate with users about model updates and prevent malicious activity.

On the software download page, you will note the existence of two links to database (DB) files. These links are updated with new database files daily at 7:00am AST. To update your local database, simple download the latest file using these links and replace the corresponding file in your model directory.

We invite the reader to please also consult the E-CHAIM Primer, submitted separately with this report, which provides detailed instructions on how to use the various E-CHAIM codes and summarizes the various features available in those codes.

References/Bibliography

Altadill, D., S. Magdaleno, J.M. Torta, and E. Blanch (2013), Global empirical models of the density peak height and of the equivalent scale height for quiet conditions, Adv. Space Res., 52, 1756-1769, doi:10.1016/j.asr.2012.11.018

Araujo-Pradere, E.A., T. J. Fuller-Rowell, and M. V. Codrescu (2002a), STORM: An empirical storm-time ionospheric correction model, 1, Model description, Radio Sci., 37(5), 1070,doi:10.1029/2001RS002467.

Araujo-Pradere, E. A., and T. J. Fuller-Rowell (2002b), STORM: An empirical storm-time ionospheric correction model, 2, Validation, Radio Sci., 37(5), 1071, doi:10.1029/2002RS002620.

Araujo-Pradere, E. A., T. J. Fuller-Rowell, M. V. Codrescu, and D. Bilitza (2005), Characteristics of the ionospheric variability as a function of season, latitude, local time, and geomagnetic activity, Radio Sci., 40, RS5009, doi:10.1029/2004RS003179.

Athieno, R., and P.T. Jayachandran (2016), MUF variability in the Arctic region: A statistical comparison with the ITU-R variability factors. Radio Sci., 51, 1278–1285, doi:10.1002/2016RS006096.

Baumjohann, W. and Y. Kamide (1984) Hemispherical Joule heating and the AE indices. J. Geophys. Res. 69, 383.

Bilitza, D., N.M. Sheikh, and R. Eyfrig (1979). A global model for the height of the F2-peak using M3000 values from the CCIR numerical map, *Telecommun. J.*, 46, pp. 549–553

Bilitza, D. (1990), International Reference Ionosphere 1990, NSSDC 90-22, Greenbelt, Maryland.

Bilitza, D., S.M. Radicella, B.W. Reinisch, J.O. Adeniyi, M.E. Mosert Gonzalez, and S.R. Zhang (2000). New B0 and B1 models for IRI. *Adv. Space Res.*, 25(1), pp. 89-95.

Bilitza, D. (2001). International Reference Ionosphere 2000. *Radio Sci.*, 36(2), pp.261-275.

Bilitza, D., and B. W. Reinisch (2008), International Reference Ionosphere 2007: Improvements and new parameters, Adv. Space Res., 42, 599–609, doi:10.1016/j.asr.2007.07.048.

Bilitza, D., L.-A. McKinnell, B.W. Reinisch, and T. Fuller-Rowell (2011). The international reference ionosphere today and in the future. *J. Geodesy* , **85**, pp. 909-920, doi: 10.1007/s00190-010-0427-x

Bilitza, D., S.A. Brown, M.Y. Wang, J.R. Souza, and P.A. Roddy (2012). Measurements and IRI model predictions during the recent solar minimum*. J. Atmos. Sol. Terr. Phys*., 86, pp. 99-106. doi: 10.1016/j.jastp.2012.06.010.

Bjoland, L.M., V. Belyey, U.P. Lovhaug, and C. La Hoz (2016), An evaluation of International Reference Ionosphere electron density in the polar cap and cusp using EISCAT Svalbard radar measurements. Ann. Geophys., 34, 751-758, doi:10.5194/angeo-34-751-2016

Bust, G. S., J. W. Garner, and T. L. Gaussiran (2004), Ionospheric data assimilation three-dimensional (IDA3D): A global multisensor, electron density specification algorithm, J. Geophys. Res., 109, A11312, doi:10.1029/2003JA010234.

Cervera, M. A., and T. J. Harris (2014), Modelling the effects of ionosphere disturbances on quasi-vertically incident ionograms using 3D magneto-ionic raytracing, J. Geophys. Res. Space Physics, 119, doi:10.1002/2013JA019247.

Ehinlafa, O. E., O. A. Falaiye, and J. O. Adeniyi (2010), Comparison of observed hmF2 and IRI 2007 model with M(3000)F2 estimation of hmF2 at low solar activity for an equatorial station, Adv. Space Res., 46, 89–93, doi:10.1016/j.asr.2010.02.018.

Ezquer, R. G., M. A. Cabrera, J. L. Lopez, M. R. Albornoz, M. Mosert, P. Marco, and D. Buresova (2011), Critical frequency and maximum electron density of F2 region over four stations in the North American sector, J. Atmos. Sol. Terr. Phys., 73, 420–429, doi:10.1016/j.jastp.2010.09.018.

Fuller-Rowell, T.J. (1998), The "thermospheric spoon": A mechanism for the semiannual density variation. J. Geophys. Res., 103(A3), 3951-3956

Foster, J.C., J.-P. St. Maurice, and V.J. Abreu (1983), Joule heating at high latitudes, J. Geophys. Res., 88, 4885-4896.

Foster, J. C., et al. (2005), Multiradar observations of the polar tongue of ionization, J. Geophys. Res., 110, A09S31, doi:10.1029/2004JA010928.

Galkin, I. A., B. W. Reinisch, X. Huang, and D. Bilitza (2012), Assimilation of GIRO data into a real-time IRI, Radio Sci., 47, RS0L07, doi:10.1029/2011RS004952.

Garner, T.W., B.T. Taylor, T.L. Gaussiran, W.R. Coley, M.R. Hairston, and F.J., Rich (2010). Statistical behavior of the topside elctron density as determined from DMSP observations: A probabilistic climatology. J. Geophys. Res., 115, A07306, doi:10.1029/2009JA014695.

George, P. L., and P. A. Bradley (1974), A new method of predicting the ionospheric absorption of high frequency waves at oblique incidence, Telecommun. J., 41(5), 307–311.

Ghezelbash, M., A. V. Koustov, D. R. Themens, and P. T. Jayachandran (2014), Seasonal and diurnal variations of PolarDARN F region echo occurrence in the polar cap and their causes, J. Geophys. Res. Space Physics, 119, 10,426–10,439, doi:10.1002/2014JA020726.

Haselgrove, J. (1963), The Hamiltonian ray path equations, J. Atmos. Terr. Phys., 25, 397–399.

Hernandez-Pajares, M., J. Juan, J. Sanz, and D. Bilitza (2002), Combining GPS measurements and IRI model values for space weather specification, Adv. Space Res., 29(6), 949–958.

Jayachandran, P. T., et al. (2009), Canadian High Arctic Ionospheric Network (CHAIN), Radio Sci., 44, RS0A03, doi:10.1029/2008RS004046.

Jones, W.B., and R.M. Gallet (1962), The representation of diurnal and geographic variations of ionospheric data by numerical methods, J. Telecommun., 29, 129-149.

Karpachev, A.T., M.V. Klimenko, V.V.Klimenko, and L.V. Pustovalova (2016), Empirical model of the main ionospheric trough for nighttime winter conditions. J. Atm. Sol.-Ter. Phys., 146, doi:10.1016/j.jastp.2016.05.008

Komjathy, A., and R. Langley (1996), Improvement of a global ionospheric model to provide ionospheric range error corrections for single frequency GPS users, Proceedings of the 52nd Annual Meeting of the Institute of Navigation, pp. 557–566, Cambridge, Mass., Jan 22-24.

Komjathy, A., R. B. Langley, and D. Bilitza (1998), Ingesting GPS-derived TEC data into the international reference ionosphere delay corrections, Adv. Space Res., 22(6), 793–801.

Lamarche, L. J., and R. A. Makarevich(2015), Solar control of F region radar backscatter: Further insights from observations in the southern polar cap, J. Geophys. Res.Space Physics, 120, 9875–9890,doi:10.1002/2015JA021663.

Lyatsky W., and A M Hamza (2001), Seasonal and diurnal variations of geomagnetic activity and their role in Space Weather forecast, Canadian Journal of Physics, 2001, 79(6): 907-920, https://doi.org/10.1139/p01-049

Makarevich, R. A., L. J. Lamarche, and M. J. Nicolls (2015), Resolute Bay incoherent scatter radar observations of plasma structures in the vicinity of polar holes, J. Geophys. Res. Space Physics, 120, doi:10.1002/2015JA021443

Pederick, L. H., M. A. Cervera, (2014), Semiempirical Model for Ionospheric Absorption based on the NRLMSISE-00 atmospheric model Radio Science, 49, 81–93, doi:10.1002/2013RS005274.

Pezzopane, M., M. Pietrella, A. Pignatelli, B. Zolesi, and L. R. Cander (2011), Assimilation of autoscaled data and regional and local ionospheric models as input sources for real-time 3-D International Reference Ionosphere modeling, Radio Sci., 46, RS5009, doi:10.1029/2011RS004697.

Schmidt, M., D. Bilitza, C. Shum, and C. Zeilhofer (2008), Regional 4D modeling of the ionospheric electron density, Adv. Space Res., 42(4), 782–790, doi:10.1016/j.asr.2007.02.050.

Sethi, N. K., R. S. Dabas, and K. Sharma (2008), Comparison between IRI predictions and digital ionosonde measurements of hmF2 at New Delhi during low and moderate solar activity, J. Atmos. Sol. Terr. Phys., 70, 756–763, doi:10.1016/j.jastp.2007.10.009.

Shubin V.N. (2015), Global median model of the F2-layer peak height based on ionospheric radio-occultation and ground-based Digisonde observations, Adv. Space Res. 56, 916-928, doi:10.1016/j.asr.2015.05.029

Sojka, J. J., M. D. Bowline, and R. W. Schunk (1994), Patches in the Polar Ionosphere: UT and Seasonal Dependence, J. Geophys. Res., 99(A8), 14,959–14,970, doi:10.1029/93JA03327.

Themens, D. R., P. T. Jayachandran, M. J. Nicolls, and J. W. MacDougall (2014), A top to bottom evaluation of IRI 2007 within the polar cap, J. Geophys. Res. Space Physics, 119, 6689–6703, doi:10.1002/2014JA020052.

Themens, D.R., and P.T. Jayachandran (2016), Solar activity variability in the IRI at high latitudes: Comparisons with GPS total electron content. J. Geophys. Res. Space Physics, 121, doi:10.1002/2016JA022664.

Themens, D.R., P.T. Jayachandran, I. Galkin, and C. Hall (2017a). The Empirical Canadian High Arctic Ionospheric Model (E-CHAIM): NmF2 and hmF2, *J. Geophys. Res. Space Physics*, doi: 10.1002/2017JA024398

Themens, D.R., P.T. Jayachandran, and R.H. Varney (2017b), Examining the use of the NeQuick bottomside and topside parameterizations at high latitudes, Adv. Space Res., 68(1), doi:10.1016/j.asr.2017.09.037

Themens, D.R., et al. (2018), Topside Electron Density Representations for Middle and High Latitudes: A Topside Parameterization for E CHAIM Based on the NeQuick, Journal of Geophysical Research: Space Physics, 123, 2, 1603-1617.

Titheridge, J.E. (1985), Ionogram analysis: least-squares fitting of a Chapman layer peak. *Radio Sci.,* 20 (2), 247–256.

Titheridge, J. E. (1988), The real height analysis of ionograms: A generalized formulation, *Radio Sci.*, 23(5), 831–849.

Watson, C., P. T. Jayachandran, E. Spanswick, E. F. Donovan, and D. W. Danskin (2011), GPS TEC technique for observation of the evolution of substorm particle precipitation, J. Geophys. Res., 116, A00I90, doi:10.1029/2010JA015732.

Wichaipanich, N., P. Supnithi, T. Tsugawa, T. Maruyama, and T. Nagatsuma (2012), Comparison of ionosphere characteristic parameters obtained by ionosonde with IRI-2007 model over Southeast Asia, Adv. Space Res., 52(10), 1748–1755, doi:10.1016/j.asr.2012.06.018.

Wilkinson, P. J. (2004), Ionospheric variability and the international reference ionosphere, Adv. Space Res., 34, 1853–1859.

Zeilhofer, C., M. Schmidt, D. Bilitza, and C. K. Shum (2009), Regional 4-D modeling of the ionospheric electron density from satellite data and IRI, Adv. Space Res., 43, 1669–1675, doi:10.1016/j.asr.2008.09.033.

This page intentionally left blank.

List of symbols/abbreviations/acronyms/initialisms

DND	Department of National Defence
E-CHAIM	Empirical Canadian High Arctic Ionospheric Model
IRI	International Reference Ionosphere
NmF2	Peak density of the F2-layer
hmF2	Height of the F2-layer peak
foF2	The F2-layer critical frequency
M3000F2	Ratio of the MUF to foF2
MUF(3000)	Maximum Usable Frequency at 3000km distance
CHAIN	Canadian High Arctic Ionospheric Network
IRTAM	IRI-based Real-Time Assimilative Model
GIRO	Global Ionospheric Radio Observatory
PHaRLAP	Australian Defence Science and Technology Organisation Raytracing Toolkit
DMSP	Defense Meteorological Satellite Program
MIT	Main Ionospheric Trough
DRDC	Defence Research and Development Canada
DSTKIM	Director Science and Technology Knowledge and Information Management

DOCUMENT CONTROL DATA

*Security markings for the title, authors, abstract and keywords must be entered when the document is sensitive

1. ORIGINATOR (Name and address of the organization preparing the document. A DRDC Centre sponsoring a contractor's report, or tasking agency, is entered in Section 8.)

University of New Brunswick
8 Bailey Drive
P.O. Box 4400
Fredericton (New Brunswick) E3B 5A3
Canada

2a. SECURITY MARKING (Overall security marking of the document including special supplemental markings if applicable.)

CAN UNCLASSIFIED

2b. CONTROLLED GOODS

NON-CONTROLLED GOODS
DMC A

3. TITLE (The document title and sub-title as indicated on the title page.)

The Empirical Canadian High Arctic Ionospheric Model (E-CHAIM): Validation and Release

4. AUTHORS (Last name, followed by initials – ranks, titles, etc., not to be used)

Themens, D.; Jayachandran, P. T.; McCaffrey, A.; Reid, B.

5. DATE OF PUBLICATION (Month and year of publication of document.)	6a. NO. OF PAGES (Total pages, including Annexes, excluding DCD, covering and verso pages.)	6b. NO. OF REFS (Total references cited.)
September 2018	38	52

7. DOCUMENT CATEGORY (e.g., Scientific Report, Contract Report, Scientific Letter.)

Contract Report

8. SPONSORING CENTRE (The name and address of the department project office or laboratory sponsoring the research and development.)

Corporate Office
ADM(S&T) / DRDC Corporate
NDHQ (Carling), 60 Moodie Drive, Building 7
Ottawa, Ontario K1A 0K2
Canada

9a. PROJECT OR GRANT NO. (If appropriate, the applicable research and development project or grant number under which the document was written. Please specify whether project or grant.)	9b. CONTRACT NO. (If appropriate, the applicable number under which the document was written.)
03ba - Air Integrated – RF	W7714-186507/001/SS

10a. DRDC PUBLICATION NUMBER (The official document number by which the document is identified by the originating activity. This number must be unique to this document.)	10b. OTHER DOCUMENT NO(s). (Any other numbers which may be assigned this document either by the originator or by the sponsor.)
DRDC-RDDC-2018-C185	

11a. FUTURE DISTRIBUTION WITHIN CANADA (Approval for further dissemination of the document. Security classification must also be considered.)

Public release

11b. FUTURE DISTRIBUTION OUTSIDE CANADA (Approval for further dissemination of the document. Security classification must also be considered.)

12. KEYWORDS, DESCRIPTORS or IDENTIFIERS (Use semi-colon as a delimiter.)

Canadian High Arctic Ionospheric Model; Oblique ionospheric sounder; Ionosphere; International Reference Ionosphere; High-frequency Radar

13. ABSTRACT/RÉSUMÉ (When available in the document, the French version of the abstract must be included here.)

This phase of the E-CHAIM project involved the validation and testing of the model in preparation for final release. For this purpose, we first examined the performance of the model under the most extreme conditions one could expect it to operate (intermediate timescales). It is clear from previous work [e.g. Themens et al., 2017a] that E-CHAIM performs well and better than the International Reference Ionosphere (IRI) on monthly median timescales but little has been done to assess the model's performance at shorter timescales. Looking at intermediate (1-to- 30-day) timescales we here examine the performance of the E-CHAIM and IRI storm models in accommodating variations at these timescales. Through this work, we demonstrate that, despite the simple nature of the storm parameterization, the E-CHAIM storm model is able to account for 20%-50% of ionospheric variability at intermediate timescales. This, however, is found to be the limit of the operational capacity of empirical models, where only data assimilation can provide further improvement. To account for the lack of an independent validation of the E-CHAIM topside model in our previous work [Themens et al., 2018], we here present such a validation using Defense Meteorological Satellite Program (DMSP) in situ measurements of electron density. Through this validation we note remarkable improvement in the representation of electron density at DMSP satellite orbit altitudes over the IRI. This improvement is found to be greatest during the summer at high solar activity and can at times exceed a factor of two, while both models provide comparable performance during winter and at low solar activity. In general, E-CHAIM does an excellent job tracking the seasonal behaviour of DMSP electron density in a variety of latitude and local time domains. In order to assess the capacity of E-CHAIM to be used in HF raytracing applications, we have also applied the model with a PHaRLAP raytracing code. Using this raytracer with E-CHAIM, we note nominal behaviour with no unphysical outliers in the production of simulated vertical and oblique ionograms. Simulations of the Maximum Usable Frequency (MUF) between Resolute and Yellowknife demonstrate largely expected physical behaviour, which we hope to compare to data once available. Comparisons of E-CHAIM-derived receive power and O-mode virtual traces show largely consistent behaviour with a limited set of available oblique ionograms. Finally, we present a summary of the E-CHAIM code features released coincident with this report.

Cette phase du projet E-CHAIM comporte la validation et les essais du modèle précédant la publication de sa version définitive. Dans ce but, nous avons d'abord étudié le rendement du modèle dans les conditions de fonctionnement prévisibles les plus extrêmes, soit les échelles de temps intermédiaire. Nos travaux antérieurs (Themens et coll. 2017a) ont montré qu'aux échelles moyennes mensuelles, qu'E-CHAIM a un bon rendement et donne des résultats supérieurs à ceux de l'ionosphère internationale de référence (IIR), mais nous avons fait peu de travail pour évaluer le rendement sur des périodes plus courtes. Nous nous penchons ici sur les échelles de temps intermédiaires de un à trente jours pour étudier le comportement des modèles de tempêtes d'E-CHAIM et de l'IIR pour tenir compte des variations à ces échelles. Grâce à ce travail, nous démontrons qu'en dépit de la simplicité de la paramétrisation des tempêtes, le modèle de tempêtes d'E-CHAIM peut expliquer entre 20 % et 50 % de la variabilité ionosphérique aux échelles de temps intermédiaires. Nous avons toutefois trouvé que cette paramétrisation limitait la capacité opérationnelle des modèles empiriques qui ne pourront être améliorés que par l'assimilation de données. Étant donné l'absence d'une validation indépendante du modèle d'E-CHAIM pour le haut de la couche dans nos travaux antérieurs (Themens et coll., 2018), nous présentons une telle validation basée sur les mesures in situ de la densité d'électrons par le Defense Meteorological Satellite Program (DMSP) des États-Unis. Cette validation a permis de constater une amélioration remarquable par rapport à celle de l'IIR de la représentation de la densité d'électrons aux altitudes de l'orbite des satellites du DMSP. Nous avons trouvé que cette amélioration était plus grande pendant l'été lors de fortes activités solaires et à certains moments pouvait être d'un facteur deux. Toutefois, les deux modèles ont un rendement comparable en hiver et pendant les périodes de faible activité solaire. En général, E-CHAIM suit très bien le comportement saisonnier de la densité d'électrons trouvée par le DMSP pour un éventail de domaines de latitudes et de temps locaux. Pour évaluer la capacité

d’utilisation d’E-CHAIM avec les programmes de traçage de rayons pour les hautes fréquences, nous l’avons testé avec un logiciel de traçage de rayons PHaRLAP. Nous avons constaté que l’utilisation de ce traceur de rayons avec E-CHAIM produisait un comportement nominal sans données aberrantes non physiques lors de la production d’ionogrammes simulés verticaux et obliques. Les simulations de la fréquence maximale utilisable entre Resolute et Yellowknife montrent un comportement physique largement prévisible que nous souhaiterions comparer avec des données d’observation si elles devenaient disponibles. Les comparaisons entre les puissances reçues calculées par E-CHAIM et les traces virtuelles des ondes ordinaires montrent un comportement en accord général avec l’ensemble limité des ionogrammes obliques disponibles. Pour finir, nous présentons un résumé des éléments principaux du programme E-CHAIM, publié concurremment avec le présent rapport.